AALTO UNIVERSITY
School of Science and Technology
Faculty of Electronics, Communications and Automation
Department of Signal Processing and Acoustics

Pramod Jacob Mathecken

Performance Analysis of OFDM With Wiener Phase Noise and Frequency Selective Fading Channel

Master's Thesis submitted in partial fulfillment of the requirements for the degree of Master of Science in Technology.

Espoo, December 29, 2010

Supervisor: Professor Risto Wichman

Instructor: Taneli Riihonen, M.Sc. (Tech.)

AALTO UNIVERSITY
School of Science and Technology

ABSTRACT OF THE
MASTER'S THESIS

Author:	Pramod Jacob Mathecken
Name of the Thesis:	Performance Analysis of OFDM with Wiener Phase Noise and Frequency Selective Fading Channel
Date:	December 29, 2010 **Number of pages: 75**
Faculty:	Electronics, Communications and Automation
Department:	Signal Processing and Acoustics
Professorship:	S-88 Signal Processing
Supervisor:	Prof. Risto Wichman
Instructor:	Taneli Riihonen, M.Sc. (Tech.)

This thesis studies the effect of Wiener phase noise on the performance of orthogonal frequency division multiplexing (OFDM) systems. The main performance metrics used in the analysis are capacity and signal-to-interference-plus-noise ratio (SINR). OFDM is a multi-carrier modulation technique in which data is transmitted in parallel streams using closely spaced (in frequency) orthogonal carriers. Phase noise is the random fluctuation in the phase of the oscillator signal used in the frequency translation between baseband and radio frequency. These fluctuations occur because of the inherent imperfections in the components that make up the oscillator. With respect to OFDM, phase noise destroys the orthogonality between the carriers and this causes interference between the parallel streams of data which results in degradation of the capacity and SINR. We derive closed-form analytical expressions of average capacity and average SINR and highlight the key parameters of the phase noise process and OFDM system that affect its behavior. In comparison with previous works, a probability density function (PDF) based approach is used in arriving at these performance metrics. This approach necessitates the derivation of the PDF of a sum of gamma random variables. In earlier literature, this result is available for gamma variables that have a full-rank square-root normalized covariance matrix. We generalize the result for the rank-deficient case and apply this result to obtain the statistical expressions of capacity and SINR.

Keywords: OFDM, SINR, capacity, phase noise, common phase error, intercarrier interference, gamma distribution, power spectral density.

Acknowledgments

Behind every progress and success in our lives are those that when looked at hindsight, it would seem we would be nowhere without them. They have encouraged us, made us understand and have given a fresh perspective to life. This thesis is dedicated to those who have influenced my life.

This thesis work is an outcome of one of the many research areas of the signal processing and wireless communications group involving Prof. Risto Wichman, D.Sc. Stefan Werner, M.Sc. (Tech.) Taneli Riihonen and myself. I am immensely grateful to Prof. Risto Wichman for giving me the opportunity, freedom and responsibility to pursue on this particular area of research and in general on my interests. I cannot but thank M.Sc. (Tech.) Taneli Riihonen for formulating the problem that this thesis addresses without which this thesis probably would not have come into being. I am extremely humbled by the amount of care you have taken in going through this thesis so rigorously. Your attention to the minutest of detail, simply, never ceases to amaze me. I have learned so much from you that it truly is an enlightening and enriching learning experience. I would also like to thank D.Sc. Stefan Werner for recognizing aspects of our research that are worthy of importance and recognition which on my own i would normally overlook. Your constant emphasis on the interpretation of equations and their significance truly helps one to learn the subject in an intuitive manner and has had a profound impact on my learning. Thank you for your enthusiasm and support throughout this thesis work and making research look so much fun.

To my family, to whom i will ever so be indebted to for the rest of my life. Thank you for setting my wings free from a very young age. And finally to Satish Prabu, without whom i would have never ended up here in Finland. Thank you for your constant encouragement and making me believe in myself.

Otaniemi, December 29, 2010

Pramod Jacob Mathecken

Contents

Abbreviations

ADC	Analog to digital converter
ADSL	Asymmetric digital subscriber line
AWGN	Additive white Gaussian noise
BER	Bit error rate
BPSK	Binary phase shift keying
CDF	Cumulative distribution function
CP	Cyclic prefix
CPE	Common phase error
DAC	Digital to analog converter
DBPSK	Differential binary phase shift keying
DCT	Discrete cosine transform
DQPSK	Differential quadrature phase shift keying
DVB	Digital video broadcasting
FDMA	Frequency division multiple access
FFT	Fast Fourier transform
FIR	Finite impulse response
IEEE	Institute of Electrical and Electronics Engineers
IF	Intermediate frequency

JEN	Jitter excess noise
LAN	Local area network
MGF	Moment generating function
ML	Maximum likelihood
MMSE	Minimum mean square error
ICI	Inter carrier interference
ISI	Inter symbol interference
OFDM	Orthogonal frequency division multiplexing
PAPR	Peak to average power ratio
PDF	Probability density function
PLL	Phase locked loop
PSD	Power spectral density
PSK	Phase shift keying
QAM	Quadrature amplitude modulation
RF	Radio frequency
SC	Single carrier
SER	Symbol error rate
SINR	Signal to interference plus noise ratio
SNR	Signal to noise ratio
VCO	Voltage controlled oscillator
WLAN	Wireless local area network

List of Figures

Chapter 1

Introduction

1.1 Background

Telecommunication, by means of electrical or generically electromagnetic signals, is the act of conveying information from a sender to a receiver. It has revolutionized human civilization to such an extent that most of our modern human life would seem devoid of function without it. Our acts of watching television, listening to the radio, browsing the Internet for information, meeting friends on social networking websites, using our mobile devices to reach a destination and making travel plans are some of the most mundane activities that involve some form of telecommunication.

Telecommunication can be characterized by the physical medium or channel on which information is transmitted. Wireline communication involves transmission of signals by means of coaxial cables or waveguides. In wireless communication, the signals propagate through free space. No matter what channel we talk about, signals always undergo some form of distortion during transmission. A signal is typically characterized by its frequency response. It represents the range of frequencies required to constitute the signal. For signals to pass undistorted through a channel, the frequency response of the channel must be wider and more or less constant over the signal bandwidth.

Transmission of signals can take place in two ways. One is *baseband transmission* and the other is known as *passband transmission*. Baseband transmission implies that signal bandwidth is around the DC frequency of 0 Hertz which is transmitted through a baseband channel. In a passband transmission system, the signal to be transmitted has a bandwidth spread around a particular frequency, also known as the carrier frequency, which implies that the channel in question is also of the passband type. Typical information bearing signals to be transmitted are of the baseband type. They are upconverted to passband (or, specifically, to the carrier frequency) by the process of *modulation*, where in, the baseband

signal is multiplied with a carrier signal which is a sinusoidal signal of a certain frequency. As a result, the multiplied signal has spectrum equal to the baseband signal but is now spread around the frequency of the carrier signal.

The above paragraph on passband transmission is also described as a *single-carrier* (SC) system, i.e., the signal is transmitted by means of one and only one carrier alone. Orthogonal frequency division multiplexing (OFDM) is a *multi-carrier* transmission technique in which data is transmitted in parallel using N_c orthogonal carriers. The data to be transmitted is split into N_c parallel streams, where each stream modulates carrier signals that are orthogonal to each other and the modulated streams are combined and transmitted through the channel. The spectrum of the OFDM signal consists of overlapping frequency bands between these N_c parallel streams, unlike, in the SC case where the entire band is allocated to one carrier. The method was initially proposed in the 1950's and is currently a reality by its wide usage in many communication systems such as DAB, DVB, WIMAX, ADSL and the upcoming fourth generation LTE systems.

One of major drawbacks of SC systems is their susceptibility to the frequency selective nature of the channel. As earlier mentioned, for a signal to pass undistorted through a channel, the channel frequency response should be more or less constant over the signal bandwidth. In wide-band systems, where the signal bandwidth is large, the flat response of the channel does not hold but it instead can be highly frequency selective. Frequency selectivity distorts the signal transmitted and necessitates compensation (equalization) at the receiver. Equalization is a non-trivial task when the channel is highly frequency selective. The advantage of OFDM is that the equalization of the channel effects is simple and requires less computation. This is because data is transmitted in parallel with overlapping frequency bands, where in, each of these frequency bands occupy a narrow portion of the signal bandwidth. Over this narrow portion, the channel frequency response will more or less be constant and, hence, makes equalization a simple task.

Although OFDM has the advantage in that channel equalization is simple, it is highly sensitive, compared to SC, to radio frequency (RF) impairments that occur at the analog front-end of a communication system. RF impairments such as power amplifier non-linearities, phase noise, IQ-imbalance and jitter, cause significant degradation of performance in OFDM systems and have received significant attention in the scientific community. For example, consider phase noise; it is the random fluctuations in the phase of the sinusoidal waveform used for frequency upconversion of baseband signals to RF. This occurs due to the inherent imperfections of oscillators used for this purpose. With respect to OFDM, phase noise destroys the orthogonality of the parallel carriers and causes interference between them.

1.2 Research Problem and Scope

The scope of this thesis is in the analysis of the phase noise RF-impairment on the performance of OFDM systems. The phase noise is modeled as a Wiener process. We consider performance metrics of signal-to-interference-plus-noise-ratio (SINR) and capacity. The research problem is, thus, to determine analytical closed-form expressions of the performance metrics and, in doing so, to identify key system parameters that are critical to the performance.

1.3 Contributions of the Thesis

A plethora of earlier literature is available on the phase noise analysis of OFDM systems. The analysis is typically quantified by determining performance metrics of SINR and bit error rates (BER). A missing aspect in the literature related to phase noise for OFDM is the evaluation of the capacity. Thus, we choose the capacity as one of our performance metrics and derive closed-form expressions for it. Most of the approaches in evaluating the average SINR are based on obtaining second order statistics to the variables in question. In this thesis, we use a probability density function (PDF) based approach for evaluating the average capacity, average SINR and outage capacity. Knowledge of this PDF facilitates an accurate estimate of the average measures of performance metrics. An outcome of this thesis is a journal article which is soon to be published [28].

The main contributions are summarized as follows

- We use a PDF-based approach for obtaining the average capacity and SINR of OFDM systems impaired by phase noise.
- We show that the instantaneous SINR and capacity are characterized by two random variables, one describing the phase noise process and the other representing the channel. Using a Taylor series approximation, we show that the random variable, characterizing Wiener phase noise, can be expressed as a sum of correlated gamma random variables.
- We derive the PDF of a sum of correlated gamma random variables. A similar result was derived in [2]. However, their PDF is applicable only when the square-root of the normalized covariance matrix of the gamma variables is full-rank while the correlated gamma variables in our case have a rank-deficient square-root normalized covariance matrix. We generalize the earlier result for the rank-deficient case.

1.4 Outline of the Thesis

The remainder of the thesis is organized as follows. In Chapter 2, we conduct a literature study of phase noise effects on OFDM. We cover both aspects: analysis of its effects on OFDM and compensation methods to negate its undesired effects. Although the phase noise process dealt in this thesis is of the Wiener type, we also dwell briefly into phase noise modeling. In general Chapter 3 presents the OFDM system model in the presence of phase noise. We derive expressions for instantaneous SINR and show its dependence on two random variables, one characterizing the phase noise process and the other the fading channel. We show in Chapter 4, that the random variable characterizing Wiener phase noise, in the SINR expression, is a sum of correlated gamma random variables whose PDF we derive. With the PDFs describing the channel and the phase noise process at hand, we proceed in the Chapter 5 to derive closed-form statistical expressions of capacity and SINR. In Chapter 6, we compare our analytical results with the simulations and analyze key parameters that affect the behavior of the performance metrics. We finally conclude in Chapter 7.

Chapter 2

Recent Advances in OFDM Impaired by Phase Noise

In this chapter, we summarize much of the work that has been done on OFDM affected by phase noise. We begin by a brief treatise on what OFDM is, its benefits and drawbacks. The drawbacks are mainly to do with RF impairments such as frequency offset, phase noise, IQ imbalance and power amplifier nonlinearities. As phase noise is in the focus of this thesis, we discuss first the characterization of phase noise processes in Section 2.3. The literature of phase noise related to OFDM can be classified into two kinds. One is analysis of the effects of phase noise in OFDM and the other is about compensation techniques. The performance analysis measures are typically signal-to-noise-plus-interference ratio (SINR) and bit error rates (BER). We review work on the analysis methods in Section 2.4. The compensation techniques typically deal with signal processing algorithms that compensate the effect of phase noise at the receiver end of a communication link. The final section of this chapter is focused toward some of these compensation techniques.

2.1 OFDM

OFDM (Orthogonal Frequency Division Multiplexing) [52,60] is a multi-carrier modulation technique in which N_c parallel data streams are transmitted in N_c orthogonal carriers. In the conventional single carrier modulation system, the entire bandwidth is allocated to one single carrier on which the baseband user signal is modulated. In OFDM, the same bandwidth is divided among N_c *overlapping* orthogonal carriers called as *subcarriers*. Figure 2.1 compares the frequency domain representation of both these systems. For the figure shown, the number of subcarriers is $N_c = 5$ for the OFDM system. In a single carrier system, each user is alloted a bandwidth equivalent to the bandwidth alloted for N_c

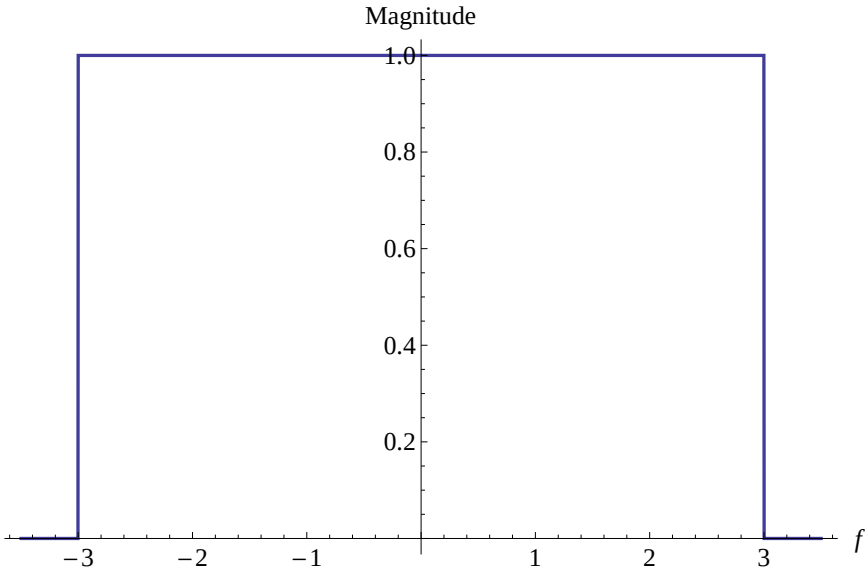

(a) Single carrier system.

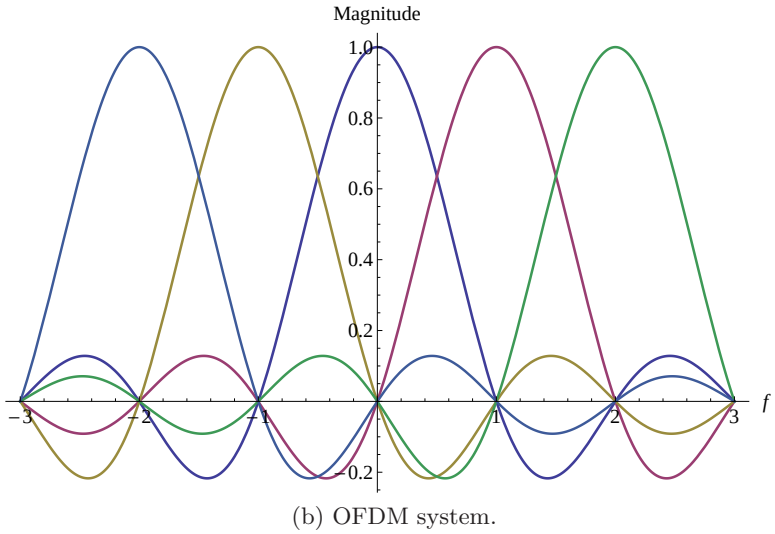

(b) OFDM system.

Figure 2.1: Comparison between single carrier and OFDM systems.

orthogonal subcarriers in an OFDM system. There are many ways of multiplexing user data in an OFDM system. One method is to allocate all the subcarriers to one particular user while the other assigns to each user a particular subcarrier. One can always speculate that for the same bandwidth as in the single-carrier case, the capacity for the OFDM system would be higher compared to its single carrier counterpart as we have N_c parallel data streams. However, this is not the case as the bandwidth in both the cases are the same and by Shannons capacity theorem, the net throughput depends on the available bandwidth.

The motivation for switching toward OFDM is multi facet. One of the major pluses for using OFDM has to do with how it sees the channel. As data is independently multiplexed on orthogonal subcarriers with a certain subcarrier spacing, each subcarrier when it passes through the channel will more or less see a channel that is flat faded. The frequency response of a channel is typically characterized by its coherence bandwidth [42, Chapter 14]. The coherence bandwidth specifies the range of frequencies over which response is more or less flat. Thus, if the subcarrier spacing is small compared to the coherence bandwidth, then each subcarrier of the OFDM signal will see a flat faded channel. In most practical cases, the coherence bandwidth is in the order of hundreds of kilo Hertz and the subcarrier spacing for most OFDM systems is about a few tens of kilo Hertz. Contrast this to the single carrier case, where the user signal is spread across the entire bandwidth of the transmitted signal which then sees a frequency selective channel.

A consequence of the flat faded channel seen by the orthogonal subcarriers is that equalization becomes a trivial task at the receiver. An equalizer tries to invert the effects of what a channel does to the transmitted user signal. Now because, each subcarrier sees a flat faded channel, equalization is easily implemented in the frequency domain by a single tap FIR filter (scalar gain) which simplifies complexity and equalizer design.

Low complexity in the generation of the OFDM signal is another major factor as to why OFDM has become so popular. The use of the discrete Fourier transform (DFT) and its extremely efficient and well established FFT algorithms for implementation has made OFDM amenable, in terms of cost, to many of the telecom operators and device manufacturers that it has been incorporated in numerous standards and systems that we encounter today.

A typical OFDM signal is transmitted by means of frames in which each frame is composed of a certain number of OFDM symbols. Now, because of the multi-path nature of the channel, the received signal is corrupted by intersymbol interference, i.e., successive OFDM symbols overlap in time. To combat this effect, an additional and sufficient amount of samples (guard interval) is appended to the OFDM symbol. At the receiver side, after passing through the channel, the OFDM symbols do not overlap in time (the effect of multipath is still experienced within each symbol) and this additional amount of samples can then discarded before retrieving the useful data. There are many ways of choosing the guard interval and each has its own benefits. The typical guard interval used in OFDM is the cyclic prefix. Its name derives from the fact that it is the last few samples of the OFDM symbol prefixed at the beginning of the OFDM symbol. Clearly, the length of the cyclic prefix depends on the nature of the multipath channel and should be long enough to capture the entire effect of the channel, i.e., it should be longer than the number of channel taps. The drawback with a long cyclic prefix is the net reduction in the throughput. To

counter this effect, the number of subcarriers has to be large in comparison with the cyclic prefix length.

2.2 Susceptibility of OFDM to RF Impairments

One of major drawback of OFDM is its sensitivity to the RF impairments that typically occur at the analog front-end of an RF communication chain [13]. RF impairments such as IQ imbalance, carrier frequency offset, phase noise, power amplifier non-linearities have all been shown to have considerable negative impact on the performance of systems employing OFDM. In this section, we briefly describe the effects that each of these impairments have on OFDM.

2.2.1 IQ Imbalance

IQ imbalance is the amplitude and phase mismatch of the oscillator signals used for mixing the in-phase and quadrature components of the input signal [24, 62, 63]. These arise due to limitations in the accuracy of the hardware used in the generation of these signals. Any typical real transmitted signal would have its spectrum centered around the carrier frequency. In the absence of IQ imbalance, at the receiver side, during the conversion from RF to baseband, the spectrum of the transmitted signal is translated to baseband with the spectrum now being symmetric around the origin. However, in the presence of a mismatch, the spectrum above and below the carrier frequency of the transmitted signal overlap with each other after downconversion. In the case of OFDM because of the two overlapping spectra (from the positive and negative side w.r.t.the carrier), each subcarrier experiences interference from its symmetric counterpart.

The origin of IQ imbalance has to do with image rejection architectures proposed for heterodyne receivers [45]. Heterodyne receivers are highly prone to image frequencies especially when employing multiple intermediate frequency (IF) stages in the RF chain. Image rejection architectures basically consist of splitting the input path into an in-phase and quadrature-phase paths and in the ideal case of no mismatch, the image signal is removed. However, most transceivers today are of the direct-conversion type, i.e., no IF stage is employed and direct conversion from RF to baseband is done. For these type of receivers, i.e., no IF stage, the image signal does not arise and is not the main consideration.

2.2.2 Frequency Offset and Phase Noise

Frequency offset and phase noise are two of the major deterrents to the amount of capacity a communication system can achieve [15, 39, 41, 56] and, hence, the development of efficient

and low complexity signal processing algorithms is crucial to mitigate their effect [32,33,53], especially given cost constraints. Frequency offset and phase noise create the same effect on the signal with the fundamental difference being that frequency offset is deterministic while phase noise is random. Frequency offset is the frequency mismatch between the incoming RF signal impinging the receiver and receiver oscillator used to down convert the RF signal to IF frequency or baseband frequency. This can arise out of two situations.

- Frequency mismatch between the transmit and receive oscillators.
- Time variations in the channel causes the transmitted RF frequency to vary in time which is popularly known by the phenomena of Doppler shift.

Phase noise on the other hand is random perturbations in the phase of the carrier signal generated by the oscillators. An ideal oscillator will generate a pure complex sinusoid of a particular frequency also called carrier frequency, i.e., $a(t) = e^{\jmath 2\pi f_c t}$ whose spectrum is characterized by an impulse function located at the frequency f_c. In the presence of phase noise or frequency offset, the oscillator output can be written as $a(t) = e^{\jmath(2\pi f_c t + \theta(t))}$. In the case of frequency offset, $\theta(t) = f_v t$, where f_v denotes the offset. Thus, the spectrum of the oscillator output is still an impulse function located at frequency $f_c + f_v$ rather than at f_c. With phase noise, $\theta(t)$ is a random process. The output of the oscillator can, thus, be viewed as a multiplication of the complex sinusoid with the function $e^{\jmath\theta(t)}$, which, in the frequency domain, results in convolution of the impulse function located at f_c with the spectrum of the signal $e^{\jmath\theta(t)}$. The net effect being the spectrum of $e^{\jmath\theta(t)}$ is translated by f_c. For most practical oscillators, $\theta(t)$ is generally a low pass process and, hence, the oscillator output spectrum would be a narrow band around the carrier frequency which can be seen as a spreading of the impulse function. This effect is demonstrated in Fig. 2.2.

In the previous paragraph, we described the spectrum of the oscillator output corrupted by offset or phase noise. It is also important to see the effects of these impairments on the input signal itself, especially on an OFDM signal. Let us first consider frequency offset. At the receiver side after down conversion and in the presence of an offset, the received baseband signal is multiplied with a complex sinusoid of frequency equal to the offset. This is equivalent to convolving the spectrum of the received signal with the spectrum of a windowed complex sinusoid (it is windowed because of the finite duration of the received signal) which is the sinc function (frequency response of a rectangular pulse) centered around the offset frequency. In OFDM, because data (drawn from a particular constellation, e.g., QAM, PSK etc.) is transmitted on parallel orthogonal subcarriers, each subcarrier will now experience interference from neighboring subcarriers because of the convolution operation in the frequency domain. Similarly, in the case of phase noise, the spectrum of the OFDM signal is convolved with the complex exponential of the low pass phase noise process (which is

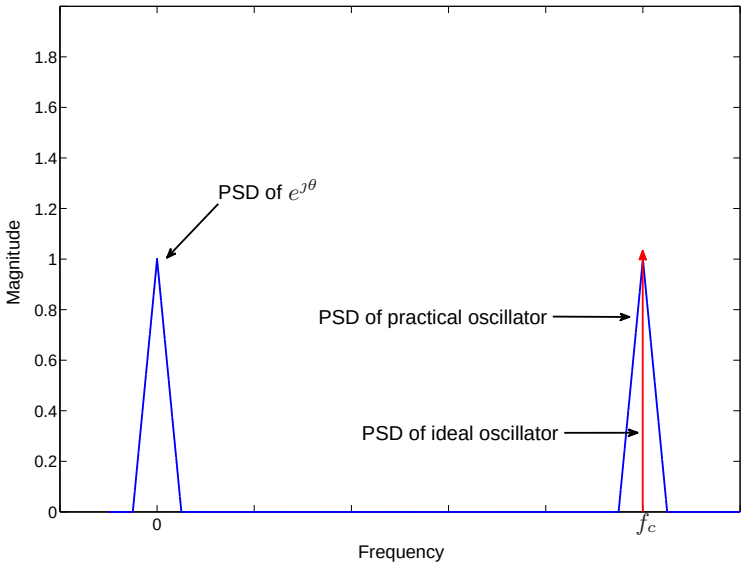

Figure 2.2: Comparison between power spectral density (PSD) of ideal and practical oscillators.

still a low pass process) and, hence, results in interference from the neighboring subcarriers. Ultimately, this causes a rotation and noise like blurring of the signal constellation which are termed as common phase error (CPE) and inter-carrier-interference (ICI) respectively [57].

2.2.3 Power Amplifier Non-Linearities

Power amplifier is an indispensable component in any telecommunication system. Power amplifiers are typically used for boosting the signal power before transmission. However, power amplifiers are inherently non-linear which result in distortion of the input signal. The situation becomes worse with OFDM because of its large signal dynamics. OFDM signals are characterized by having a large peak-to-average-power-ratio (PAPR) and will experience clipping when passed through the power amplifier (because of the saturation level of the power amplifier). This introduces in-band distortion and out-of-band spectral regrowth [7, 9].

One way of overcoming the distortion effects of the power amplifier is to simply use a linear power amplifier with high signal dynamics which would inherently increase the cost of the RF front end. Another method is to operate the non-linear power amplifier at a high input back off (defined as the ratio of the saturation power of the power amplifier to the input signal power), so that the signal experiences the linear region of the amplifier. However, this decreases the efficiency of the amplifier. The above two methods are not

practical, in terms of cost, and, hence, signal processing techniques are used to overcome the distortion effects. One of the most popular methods is to use a pre-distorter at the transmitter prior to amplification [5]. The pre-distorter is designed in such a way that the combined effect with the power amplifier makes the input signal to always see a linear region. However, this requires accurate modeling of amplifier non-linearities. Another method is to clip the OFDM signal to reduce the PAPR, so that it experiences the linear region of the power amplifier. At the receiver side, the goal is to undo the effect of clipping done at the transmitter [13] where it is assumed that the receiver has knowledge of the clipping function used at the transmitter.

2.2.4 Jitter

Jitter is the random fluctuation in the sampling instants at which a continuous-time signal is converted to a digital signal [13]. The sampling process is typically done by analog-to-digital converters (ADC). Jitter causes the ADC to sample at incorrect instances, thereby, corrupting the output signal. Jitter can occur in two ways depending upon how the sampling operation is performed. Aperture jitter is due to the noise that occurs in the sample and hold circuitry of the ADC. If the sampling operation is done by means of an external clock generated by an oscillator then the jitter is due to the phase noise inherent in the oscillator.

One of the straightforward ways of reducing the effect of jitter is to design better quality ADCs. ADC performance is typically characterized by its resolution (number of bits per sample) and SNR [59]. The effect of jitter is decreased SNR and resolution of the ADC, especially, for high sample rates for which it is more pronounced. The other scheme is to employ digital signal processing methods to compensate the effects of jitter at the receiver. With respect to OFDM, it is shown in [43], that jitter causes two effects:

- it introduces phase noise whose effect is manifested in the form CPE and ICI.
- it introduces waveform noise whose effect is to cause additive interference termed as jitter excess noise (JEN).

Thus, the compensation of jitter in OFDM consists of estimating the CPE and ICI induced by the phase noise process for which existing phase noise mitigation techniques can be used. However, the estimation of JEN is still to be investigated.

2.3 Modeling of Phase Noise

Oscillators form one of the key components in any communication system and more broadly in any digital system. In most digital systems, oscillators are typically used for timing

synchronization. However, w.r.t. analog transmissions through the channel, their use for frequency translation between baseband and RF is unique.

An ideal oscillator generates a pure sinusoid which is used to modulate the baseband signal. A complex representation of such a signal is

$$a(t) = Ae^{\jmath 2\pi f_c t}, \tag{2.1}$$

where f_c denotes the frequency of oscillation and A is the amplitude of the complex tone. The frequency translation of the input signal to RF takes place by multiplying it with oscillator signal $a(t)$. However, because of inherent imperfections in oscillators [47], a practical oscillator output signal will be of the form

$$a(t) = A(1 + \alpha(t))e^{\jmath(2\pi f_c t + \theta(t))}, \tag{2.2}$$

where the respective $\alpha(t)$ and $\theta(t)$ denote the amplitude and phase modulation of the carrier. These amplitude and phase modulating signals are termed as amplitude and phase noise respectively. The effect of these undesirable quantities is shown in Fig. 2.2. In the figure, we have ignored the amplitude noise which in general is quite small. The spreading of the oscillator spectral density due to phase noise causes interference from neighboring channels in single carrier systems and interference between sub-carriers in OFDM (multi-carrier) [41]. Thus, in order to understand its impact on the performance of communication systems accurate modeling of phase noise processes is essential [26].

The characterization of phase noise is typically done in the frequency domain by analyzing its PSD. The power law model for the PSD of the phase noise is the most widely used and has been found to closely match with measurements of most practical oscillators [3, 47, 48]. This power law model is given below as

$$S_\theta(f) = \sum_{i=0}^{4} \frac{h_i}{f^i}, \tag{2.3}$$

where $S_\theta(f)$ denotes the PSD of the phase noise process $\theta(t)$ and the coefficients h_i depend on the specific oscillator used. For most oscillators, high slopes of PSD (e.g., $1/f^4$ or $1/f^3$) occur for values of f close to the carrier frequency while lower slopes of flicker noise ($1/f$) and white noise ($1/f^0$) occur at large frequency offsets from the carrier frequency. A typical plot in the log scale is shown in Fig. 2.3. Thus, we observe from the figure that steep slopes of the PSD correspond to the low offset frequencies and high frequencies are associated with less steep ones. However, not all of terms are present in (2.3). For example, in two port devices, the phase noise PSD cannot be steeper than $1/f$ [47]. Although, the exponents

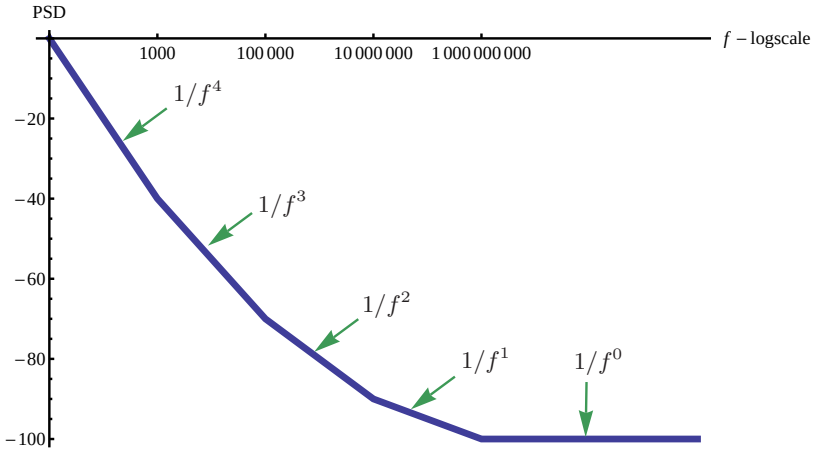

Figure 2.3: Phase noise power spectral density

in the power model take integer values, in practice these are non-integer values that can be approximated to the nearest integer. From (2.3), a common method used to estimate the phase noise process would be to pass white Gaussian noise as input to a linear-time-invariant filter such that PSD of the output filter matches closely with measured PSD of the phase noise [15]. Although, the PSD of the phase noise is crucial to understanding its effect on communication systems, it is the PSD of the oscillator output that is generally used as a measure of its spectral purity. A general expression relating the PSD of the phase noise and the oscillator PSD of (2.2) can be found in [48].

The above power law model of the PSD of phase noise, that is widely used in the literature, is typically obtained by applying either linear time invariant or time variant techniques to the oscillator in question [11]. Although, these methods provide a simple and easy understanding on the behavior of phase noise in oscillators, fundamental issues like infinite power of the oscillator PSD at the zero offset frequency which the method predicts do not hold in practice. In their seminal works [10, 11], the authors undertake a radical approach to understand the behavior of phase noise on open loop oscillators and oscillators with feedback. By considering a general model for the oscillator [11], the authors use non-linear perturbation analysis for the noisy oscillator, where the noise contributions, from different components that make up the oscillator, are modeled as white Gaussian noise sources. The authors show that asymptotically, the phase noise becomes a Brownian motion or Wiener process and the oscillator PSD follows a Lorentzian spectrum (see (3.29) of Chapter 3). In [10], the authors generalize the approach for a combination of white and colored Gaussian noise sources that arise in the different components that make up the oscillator. They show that the oscillator PSD, for frequencies close to the carrier, becomes essentially a Lorentzian spectrum while for large frequency offsets, the white noise sources cause a $1/f^2$

fall and the colored noise sources cause $1/f^2$ fall multiplied with the spectral density of the colored noise sources (implies that the colored noise sources are stationary processes).

Building on the foundations of the principles used in [10, 11], the analysis in [29] focuses on phase noise for closed-loop oscillators or phase-locked loops (PLL). A typical PLL compares the phase of the voltage-controlled oscillator (VCO) with a reference oscillator whose difference, after filtering through a loop filter, is used to control the VCO input. As the reference signal is not part of the loop, the phase noise of the reference oscillator is modeled as Brownian motion. By taking into account various noise sources (modeled as white Gaussian processes) in the PLL (the loop filter, the phase comparator and the components that make up the VCO), the authors show the resulting phase noise of the VCO output is a sum of two stochastic processes. One is the Wiener phase noise process of the reference oscillator and the other is a Ornstein-Uhlenbeck process [16]. The author also shows that the output PSD of VCO output, for low offset frequencies, follows the PSD of the reference oscillator while for large offsets the PSD follows the spectrum of the open loop VCO output.

2.4 Performance Analysis

In this section, we briefly review much of the literature related to analyzing the effect of phase noise on OFDM. We more or less use a time-line approach in reviewing the literature. In earlier literature, the phase noise effects are typically measured in terms of the signal-to-noise-plus-interference (SINR) ratio and bit-error rate (BER) or symbol error rate (SER).

The initial work by Pollet et al. in [41] shows that OFDM is more sensitive to frequency offset and phase noise when compared to its single-carrier counterpart. They derive the degradation in the SINR for the single and multi-carrier (OFDM) case. For the frequency offset and phase noise, the degradation, for single and multi-carrier, is proportional to the offset and the 3dB bandwidth of the phase noise process (assuming a Wiener phase noise model), respectively. However, a larger degradation for OFDM comes from the fact that, the degradation is also proportional to the number of subcarriers.

In [58], Tomba provides BER analysis for Wiener phase noise impaired OFDM with four modulation schemes namely, BPSK, QPSK, DBPSK and DQPSK with DBPSK performing the best. Although analytical expressions of the BERs are derived, they need to be evaluated numerically and clear insight is not obtained into the behavior of phase noise on BER curves from the expressions. Another drawback with the above analysis is the assumption of independence between the CPE and ICI, and also the Gaussianity assumption of the ICI which is not necessarily true [51].

In [50], Santhanathan and Tellambura derive the probability of symbol error conditioned on a fixed realization of the phase noise process. Since frequency offset is a deterministic

case of phase noise, the conditional probability becomes the exact symbol error probability. However, for phase noise, the symbol error probability is a random variable and to obtain its average, we need to average over the distribution of the DFT of the phase noise process.

In [15], Armada discusses how high phase noise levels can be tolerated if proper phase noise correction schemes are employed. The phase noise model is described by passing white Gaussian noise through a lowpass filter that accurately matches the power spectral density (PSD) of the phase noise. As expected the SINR degradation is larger for high phase noise levels implying a larger passband cutoff frequency of the lowpass filter. After applying a CPE correction scheme, we would expect that SER decreases. This is valid only when passband cutoff is well within the subcarrier spacing as the CPE is the dominant factor contributing to high SER and degradation. For high phase noise levels, the ICI is dominant and just CPE correction does not improve the SER. Thereby, employing proper correction schemes in order to achieve a target SER and SINR, tolerable phase noise levels can be allowed at the oscillators which reduces costs.

In [49], the authors use a non-linear (cf. linear in previous works) approximation of phase noise. The authors derive the SINR and its degradation and show how previous works of SINR degradation are special cases of the non-linear approximation method, thereby being more applicable to high phase noise levels. However, the approximation is only up to the second-order polynomial. The work by Wu and Bar-Ness in [56] generalizes the analysis to any phase noise level while also considering a multi-path fading channel unlike AWGN channels in previous literature. Clear insight is obtained from the closed-form SINR expressions that the degradation depends on the subcarrier spacing and 3dB bandwidth of the phase noise process. However, the analysis is for Wiener phase noise.

In [4], Bittner et al. provide a semi-analytical approach for evaluating the SER and capacity. The analysis includes impairments of phase noise and power amplifier non-linearities while also considering channel estimation errors. They derive the PDF of the decision variable, which is the input to the detector, conditioned on a fixed transmitted symbol and fixed realization of the DFT of phase noise. Thus, given the PDF, one can evaluate the probability of correct decision and hence the symbol error probability. However, the PDF is first averaged over the distribution of the DFT of the phase noise which is then used in the error probability calculations. This averaging is done numerically as so far there is no know closed-form expression for the joint PDF of the DFT of the phase noise. The throughput is also evaluated from the PDF of the decision variable [61].

One of the major controversies with regard to phase noise in OFDM is the characterization of the distribution of the ICI. In evaluating the BER and SER, most previous works assume a Gaussian distribution for the ICI when the number of subcarriers is very large. Because the ICI is composed of interference from other subcarriers, then by the central limit

theorem, if the number of subcarriers is large then the resulting distribution tends toward a Gaussian distribution. However, some of the work in [37, 38, 51] clearly demonstrate that this does not hold even when the number of subcarriers is large. This is because the ICI is mainly composed of interference from the neighboring subcarriers because typical phase noise processes are low-pass processes and practically zero interference occurs from far away subcarriers. Hence, the central limit theorem no longer holds. In [38], the authors derive two ways of computing the ICI power. One is by using the correlation matrix between the DFTs of the phase noise process and the second is by using the PSD of the phase noise process. The analysis is applicable to both free-running oscillators (characterized by Wiener phase noise process) as well as PLL realizations. The test for Gaussianity of the ICI is done by using the kurtosis statistic which requires knowledge of the mean and variance of the ICI. For a Gaussian random variable, the kurtosis is zero and in the case of the ICI, it clearly is shown to be a positive quantity. However, for very high phase noise level, the authors show that the kurtosis approaches zero and, hence, conclude the Gaussianity of the ICI.

In [51], Schenk sheds more light into the non-validity of the Gaussian distribution by deriving the distribution of the ICI term. It is clearly shown that the ICI distribution is characterized by thicker tails when compared with the Gaussian distribution. Typical performance measures like BER and SER are characterized by the tail probabilities of the additive noise that corrupts the desired symbol. Thus, using a Gaussian approximation severely underestimates the BER and SER. Also, it is visible that the Gaussian approximation works well for very high phase noise levels or more specifically for high ratios of the 3dB bandwidth of the phase noise process and the subcarrier spacing. However, in practice, this ratio is kept much less than one, thus requiring to not assume a Gaussian distribution for the ICI.

More literature related to phase noise analysis can be found in [8,12,19,20,27,31,35,36,40, 44, 55]. In conclusion, phase noise has a detrimental effect on the performance of systems employing an OFDM modulation scheme and, thus, necessitates the use of high-quality oscillators at the transmitter and receiver. However, given cost constraints, effective compensation techniques to mitigate the effects of phase noise need to be used. In the following section, we briefly review some of the literature related to phase noise compensation.

2.5 Compensation Techniques

The problem formulation of phase noise compensation can be stated as follows. Treating the ICI as noise or more specifically Gaussian noise, the goal is to estimate the CPE which is common to all subcarriers. Most of the literature related to phase noise compensation make this assumption of Gaussianity for the ICI, which does not generally hold in practice.

For low and reasonable phase noise levels, the ICI is not Gaussian irrespective of the number of subcarriers [38]. In [39], however, the radical approach of estimating the ICI along with the CPE is undertaken.

Phase noise compensation can be broadly classified into the following types.

- Pilot based
- Non-pilot based or decision directed

In a practical OFDM system, a fraction of the total number of subcarriers is allocated for pilot data which can be used also for synchronization purposes. Pilot based schemes make use of these pilot data to estimate the CPE and ICI in a phase noise impaired OFDM system. Non-pilot based or decision directed schemes make use of past detected symbols in the estimation and suppression of phase noise. In the following paragraphs, we briefly review some of them.

Maximum-likelihood (ML) based estimation techniques are proposed in [36]. The work includes the combined effect of frequency offset and phase noise. By treating the ICI as additive Gaussian noise, the goal is to estimate the CPE which now also includes the effect of the frequency offset. By assuming that the CPE of the current OFDM symbols is a product of the CPE of the previous OFDM symbol (whose estimate is available) and a residual term, the authors derive the ML estimator for this residual component. The residual component is obtained by averaging out the rotation experienced by all the subcarriers assuming that we know the transmitted symbols. These symbols can be obtained either as pilot data (pilot based estimation) or an initial estimate of these symbols can be used for the estimation (decision directed).

A time-domain phase noise compensation algorithm is proposed in [6]. In the time domain, at each time instant, the OFDM signal is rotated by the phase noise process ($\phi[n] = e^{j\theta[n]}$), where $\theta[n]$ denotes the phase noise. Thus, in order to recover the OFDM signal, we could multiply the received signal with the conjugate of $\phi[n]$. One of the goals of the paper is, thus, to estimate $\phi^*[n]$. This is done by realizing that any time domain signal can be represented by a set of basis functions. This time domain signal is obtained by a transformation from the frequency domain to the time domain. Effectively, the authors try to estimate the frequency components of $\phi^*[n]$ using a least-squares estimator. The accuracy of the algorithm depends upon how many basis functions are used to estimate the phase noise process. The authors show that by choosing only one basis function, thereby, estimating only the DC frequency component, their estimator reduces to the ML estimate of the CPE derived in [36] (see paragraph above). The authors also compare the performance between choosing a DFT and DCT basis.

In [39], Petrovic et al. provide a very similar idea to compensate for the effect of phase noise. At the receiver side after the operation of the DFT, the received OFDM symbol is corrupted by CPE and ICI. The aim is, thus, to estimate the DFT of $\phi[n] = e^{\jmath\theta[n]}$ (which is choosing a DFT basis in [6] (see the above paragraph). However, the authors use a minimum mean square error (MMSE) estimator when compared to the least-squares estimator of [6] with the other difference being that the final compensation is done in the frequency domain. Although, the proposed method works well, the MMSE estimator used is based on the principle idea that the parameters to be estimated are drawn from a Gaussian distribution. The DFT coefficients of $\phi[n]$ are generally not Gaussian distributed random variables. Thus, knowledge of their exact distribution would improve the estimation accuracy.

In [64], Wu and Bar-Ness propose a pilot based phase noise suppression scheme for OFDM based WLANs systems. By utilizing the preambles in the IEEE 802.11a standard, the authors arrive at a MMSE estimator [22, Chapter 10] for the transmitted symbols. For the 802.11a standard, the total number of subcarriers is 64 (48 data, 4 pilot and 12 null subcarriers). The derived MMSE estimator is done for each subcarrier and requires knowledge of the channel, which is estimated by means of the preambles, the CPE and the variance of the ICI plus AWGN. The CPE is estimated by using the least-squares estimator [22, Chapter 8]. The variance of the total noise (ICI plus AWGN) term is estimated from the null subcarriers.

Another time-domain phase noise compensation method is developed in [54]. The aim is to estimate the average phase shift that occurs due to phase noise during one OFDM symbol. With this average phase shift, a linear interpolator is used to approximate the phase noise process multiplying ($\phi[n]$) the time-domain OFDM signal. This average phase shift is obtained by recognizing that the tail of the OFDM signal is the same as the cyclic prefix (i.e., the head). Thus, by correlating these two regions of the OFDM signal, an estimate for the average phase shift is obtained.

In [46], a phase noise equalization algorithm in the time domain is proposed. By linearizing the phase noise process, i.e., linear in time, estimates of the parameters of this linear model are determined for each OFDM symbol. A direct application of this linear model would be the compensation of constant frequency offset which is characterized as being linear. The parameters are determined by correlating the phase compensated symbols with the non-phase compensated symbols. Because of the dependence on the decisions of the detector, this scheme operates in a decision directed fashion and requires no prior pilot data to be known.

Chapter 3

System Model

Our starting point is to derive the OFDM system model impaired by phase noise. The aim is to derive the instantaneous SINR and hence capacity and show its dependence on the phase noise process and on the channel. An approximation to the system model is then obtained where we make use of the fact that, for most practical purposes, the 3dB bandwidth of the oscillator power spectral density is small compared to the subcarrier spacing. With the approximated system model, we go on to derive the instantaneous SINR. Simulations confirm that this approximation is well justified. We explicity show the dependence of the SINR on what we call the 'ICI power' which is a sum of the magnitude squares of the DFT of the phase noise process excluding the DC component.

3.1 Phase Noise Impaired OFDM System

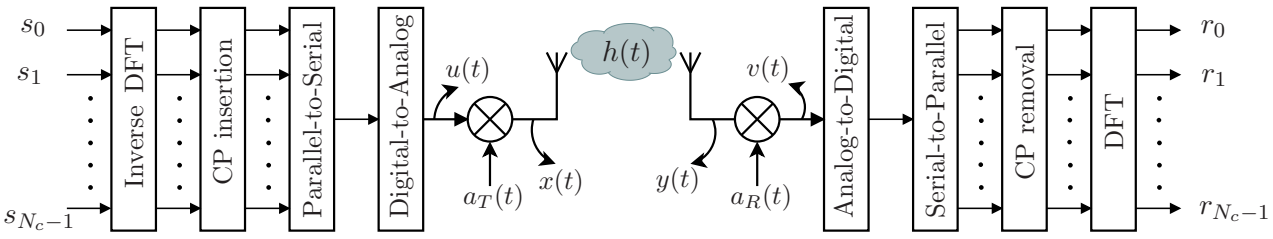

Figure 3.1: OFDM system impaired by oscillator phase noise

A typical OFDM system with N_c subcarriers is shown in Fig. 3.1. The input symbol vector $\mathbf{s}$, with elements $\{s_j\}_{j=0}^{N_c-1}$, is converted to the discrete time domain by the inverse discrete Fourier transform (IDFT) operation. Cyclic prefix is added to combat intersymbol interference followed by the parallel-to-serial and digital-to-analog conversion to obtain the baseband signal $u(t)$. We can write the discretized version, $u[n]$, of $u(t)$ using matrix

notation, in terms of the transmitted symbol vector $\mathbf{s}$ as follows

$$\mathbf{u} = \mathbf{C}_A \mathbf{F}^{-1} \mathbf{s}, \tag{3.1}$$

where $\mathbf{F}$ and $\mathbf{C}_A$ are the respective $N_c \times N_c$ DFT matrix and $N_t \times N_c$ cyclic prefix addition matrix. The cyclic prefix length is $N_t - N_c$ with N_t being the OFDM symbol length in samples. The DFT and cyclic prefix matrices are defined as

$$\mathbf{F} = \begin{bmatrix} 1 & 1 & 1 & \dots & 1 \\ 1 & W^1 & W^2 & \dots & W^{(N_c-1)} \\ 1 & W^2 & W^4 & \dots & W^{2(N_c-1)} \\ \vdots & \vdots & \vdots & \ddots & \vdots \\ 1 & W^{(N_c-1)} & W^{2(N_c-1)} & \dots & W^{(N_c-1)^2} \end{bmatrix}, \tag{3.2}$$

$$\mathbf{C}_A = \begin{bmatrix} \mathbf{0} & \mathbf{I}_{(N_t-N_c)} \\ & \mathbf{I}_{N_c} \end{bmatrix}, \tag{3.3}$$

where $W = e^{-j\frac{2\pi}{N_c}}$, the $N_c \times N_c$ identity matrix is denoted by $\mathbf{I}_{N_c}$ and $\mathbf{0}$ is an all zero matrix with dimensions $(N_t - N_c) \times (2N_c - N_t)$. This baseband signal is converted to RF by the transmit oscillator $a_T(t) = e^{j(2\pi f_c t + \theta_T(t))}$ with transmit phase noise $\theta_T(t)$ and carrier frequency f_c. The transmitted RF signal is given by

$$\begin{aligned} x(t) &= u(t) e^{j(2\pi f_c t + \theta_T(t))}, \\ &= \left(u(t) e^{j\theta_T(t)} \right) e^{j(2\pi f_c t)}. \end{aligned} \tag{3.4}$$

In the above equation, $u(t)e^{j\theta_T(t)}$ is the complex envelope [18, Appendix 2] of the bandpass signal $x(t)$. The RF signal passes through a bandpass channel $\tilde{h}(t) = h(t)e^{j2\pi f_c t}$, $h(t)$ being the complex envelope, which at the receiver is obtained as $y(t)$. Mathematically, the received RF signal can be expressed as

$$\begin{aligned} y(t) &= x(t) * \tilde{h}(t) + \tilde{n}(t), \\ &= \left(\left(u(t) e^{j\theta_T(t)} \right) * h(t) + n(t) \right) e^{j2\pi f_c t}, \end{aligned} \tag{3.5}$$

where (3.4) was used to arrive at the above equation and $\tilde{n}(t) = n(t)e^{j2\pi f_c t}$ denotes the receiver noise. The received RF signal is converted back to baseband by the receive oscillator

$a_R(t) = e^{-j(2\pi f_c t - \theta_R(t))}$, where $\theta_R(t)$ denotes the receiver phase noise. The relationship between the received RF and baseband signals is given by

$$\begin{aligned} v(t) &= y(t)e^{-j(2\pi f_c t - \theta_R(t))}, \\ &= \Big(y(t)e^{-j(2\pi f_c t)}\Big)e^{j\theta_R(t)}. \end{aligned} \tag{3.6}$$

Using (3.5) in (3.6), the received baseband signal $v(t)$ can be expressed in terms of the transmitted baseband signal $u(t)$ as follows

$$v(t) = \Big(\Big(u(t)e^{j\theta_T(t)}\Big) * h(t)\Big)\, e^{j\theta_R(t)} + n(t)e^{j\theta_R(t)}. \tag{3.7}$$

The signal $v(t)$ is converted to the discrete time domain by applying the analog-to-digital and serial-to-parallel operations to obtain $v[n]$. From (3.7), $v[n]$ can be expressed in matrix notation as

$$\mathbf{v} = \mathbf{P}_R\mathbf{G}\mathbf{P}_T\mathbf{u} + \mathbf{n}_r, \tag{3.8}$$

where $\mathbf{G}$ denotes the $N_t \times N_t$ convolution matrix of the channel and is defined as

$$\mathbf{G} = \begin{bmatrix} \boxed{h[0]} & & & \mathbf{0} \\ \vdots & \ddots & & \\ \boxed{h[L-1] \ \ldots \ h[0]} & & & \\ & \ddots & \ddots & \\ \mathbf{0} & & & \boxed{h[L-1] \ \ldots \ h[0]} \end{bmatrix}. \tag{3.9}$$

The impulse response $h[n]$ is the discrete time equivalent of the complex envelope $h(t)$ of the channel. The noise vector is given by $\mathbf{n}_r$ whose elements are the discrete version of $n(t)e^{j\theta_R(t)}$. The $\mathbf{P}_T$ and $\mathbf{P}_R$ diagonal matrices with dimensions $N_t \times N_t$ are defined below as

$$\mathbf{P}_X = \text{diag}\left[e^{j\theta_X[mN_t]} \ e^{j\theta_X[1+mN_t]} \ \ldots \ e^{j\theta_X[N_t-1+mN_t]}\right], \tag{3.10}$$

where the integer m refers to the m^{th} OFDM symbol.

The signal $v[n]$ is converted to the discrete frequency domain by applying the DFT operation, before which the cyclic prefix is removed, to obtain the received symbol vector $\mathbf{r}$ with elements $\{r_j\}_{j=0}^{N_c-1}$ as shown in Fig. 3.1, i.e.,

$$\mathbf{r} = \mathbf{F}\mathbf{C}_R\mathbf{v}, \tag{3.11}$$

where $\mathbf{C}_R$ is the $N_c \times N_t$ cyclic prefix removal matrix and is defined as

$$\mathbf{C}_R = [\mathbf{0} \;\; \mathbf{I}_{N_c}]\,. \tag{3.12}$$

Substituting (3.8) and (3.1) in (3.11), the expression relating $\mathbf{r}$ and $\mathbf{s}$ can be derived to obtain the equation below

$$\begin{aligned} \mathbf{r} &= \mathbf{F}\mathbf{C}_R\mathbf{P}_R\mathbf{G}\mathbf{P}_T\mathbf{C}_A\mathbf{F}^{-1}\mathbf{s} + \mathbf{F}\mathbf{C}_R\mathbf{n}_r, \\ &= \mathbf{F}\mathbf{C}_R\mathbf{P}_R\mathbf{C}_A\mathbf{F}^{-1}\mathbf{H}\mathbf{F}\mathbf{C}_R\mathbf{P}_T\mathbf{C}_A\mathbf{F}^{-1}\mathbf{s} + \mathbf{n}, \\ &= \mathbf{V}\mathbf{s} + \mathbf{n}. \end{aligned} \tag{3.13}$$

In arriving at (3.13), we made use of the fact $\mathbf{C}_R\mathbf{G}\mathbf{C}_A = \mathbf{F}^{-1}\mathbf{H}\mathbf{F}$, i.e., the matrix $\mathbf{C}_R\mathbf{G}\mathbf{C}_A$ is circulant and hence is diagonalizable by the DFT matrix [14]. The elements of the diagonal $N_c \times N_c$ $\mathbf{H}$ matrix are N_c point DFTs of $h[n]$. It is defined as

$$\mathbf{H} = \text{diag}\left[H_0 \; H_1 \; \ldots \; H_{N_c-1}\right], \tag{3.14}$$

where $H_l = \sum_{n=0}^{L-1} h[l]e^{-j\frac{2\pi nl}{N_c}}$, $l = 0, 1, \ldots, N_c - 1$. From the definition of the DFT, cyclic prefix, $\mathbf{P}_T$, $\mathbf{P}_R$ and $\mathbf{H}$ matrices, the matrix $\mathbf{V}$ in (3.13) can be derived to be obtained as

$$\mathbf{V} = \begin{bmatrix} \sum_{i=0}^{N_c-1} \delta_i^R H_i \delta_{-i}^T & \sum_{i=0}^{N_c-1} \delta_i^R H_i \delta_{-i+1}^T & \ldots & \sum_{i=0}^{N_c-1} \delta_i^R H_i \delta_{-i+N_c-1}^T \\ \sum_{i=0}^{N_c-1} \delta_{i-1}^R H_i \delta_{-i}^T & \sum_{i=0}^{N_c-1} \delta_{i-1}^R H_i \delta_{-i+1}^T & \ldots & \sum_{i=0}^{N_c-1} \delta_{i-1}^R H_i \delta_{-i+N_c-1}^T \\ \vdots & \vdots & \ddots & \vdots \\ \sum_{i=0}^{N_c-1} \delta_{i-N_c+1}^R H_i \delta_{-i}^T & \sum_{i=0}^{N_c-1} \delta_{i-N_c+1}^R H_i \delta_{-i+1}^T & \ldots & \sum_{i=0}^{N_c-1} \delta_{i-N_c+1}^R H_i \delta_{-i+N_c-1}^T \end{bmatrix}, \tag{3.15}$$

where $\delta_i^X = \frac{1}{N_c}\sum_{n=mN_c}^{N_c(m+1)-1} e^{j\theta_X[n]}e^{-j2\pi in/N_c}$, $X \in \{T, R\}$, is the N_c point DFT of $e^{j\theta_X[n]}$ and m refers to the mth OFDM symbol, i.e., $m = 0, 1, \ldots$. The discrete-time equivalent of $\theta_X(t)$ is given by $\theta_X[n]$. With the $\mathbf{V}$ matrix defined above, the j^{th} received subcarrier is given by

$$r_j = \Big(\sum_{i=0}^{N_c-1} \delta_{i-j}^R H_i \delta_{-i+j}^T\Big)s_j + \sum_{k=0,k\neq j}^{N_c-1} \Big(\sum_{i=0}^{N_c-1} \delta_{i-j}^R H_i \delta_{-i+k}^T\Big)s_k + n_j. \tag{3.16}$$

The white Gaussian receiver noise is denoted by n_j with variance σ_n^2.

From (3.16), we see that the transmitted data s_j on the j^{th} subcarriers phase rotated which is called the common phase error (CPE) along with unwanted interference from other subcarriers with data s_k termed as intercarrier interference (ICI). In the absence of phase noise, i.e., $\theta_X[n] = 0$, $\forall\, n$, hence $\delta_i^X = 1$ only for $i = 0$ and zero elsewhere, and $\mathbf{V}$, thus,

reduces to a diagonal matrix of elements H_i, $i = 0, 1, \ldots, N_c - 1$. This is easily visualized in Fig. 3.2a which shows the spectrum of an OFDM signal with three orthogonal subcarriers. Note the subcarriers are not the dirac delta functions but sinc functions ($\text{sinc}(x) = \frac{\sin(\pi x)}{\pi x}$), because of the rectangular time window that is used to obtain one OFDM symbol in the time domain. These sinc functions would be weighted by transmitted symbols s_j at the transmitter end. For simplicity and ease of understanding, we have neglected the effect of the channel in the figure. Clearly at the DFT sampling instants, there is no interference from other subcarriers. The scenario does not change even when we have a channel (provided the Doppler bandwidth is small) except that the DFT sampling instants are weighted by the channel frequency response. Contrast the case when we have phase noise and the spectrum would look as in Fig. 3.2b. We see from the figure that at the DFT sampling instants, each subcarrier is affected by the sidelobes from other subcarriers, with larger interference from neighbouring subcarriers compared with subcarriers that are further apart.

3.2 Approximation to the System Model

The weights of the symbols in (3.16) represent the output of a circular convolution operation of $(\delta^R_{i-j} H_i) * \delta^T_i$. In the absense of phase noise, the PSD of the oscillator will have only a spectral component at the carrier frequency. However, this is an idealistic scenario and most practical oscillators, because of phase noise, will see the spreading of its PSD (nonzero δ^X_i), around the carrier frequency, whose power decreases with increasing frequency. The amount of spread is characterized by the 3dB bandwidth of the PSD. For most oscillators, the 3dB bandwidth is small compared with the subcarrier spacing f_{sub}. Thus, δ^R_{i-j} has its maxima at $i = j$ and the power decreases rapidly around this frequency and we may approximate

$$\delta^R_{i-j} H_i \approx \begin{cases} 0 & \text{for large } i-j \\ \delta^R_{i-j} H_j & \text{for small } i-j \end{cases}$$

i.e., the channel is coherent around the frequency $i = j$. This is a reasonable assumption as the main lobe of the PSD for most oscillators is in the order of a few kiloHertz which is well within the coherence bandwidth of most channels. Consequently, we can approximate the weights as follows

$$(\delta^R_{i-j} H_i) * \delta^T_i \approx H_j \left(\delta^R_{i-j} * \delta^T_i \right) = H_j \delta_{i-j}, \tag{3.17}$$

where

$$\delta_{i-j} = \frac{1}{N_c} \sum_{n=mN_c}^{N_c(m+1)-1} e^{j(\theta^T[n] + \theta^R[n])} e^{-j(2\pi(i-j)n)/N_c}. \tag{3.18}$$

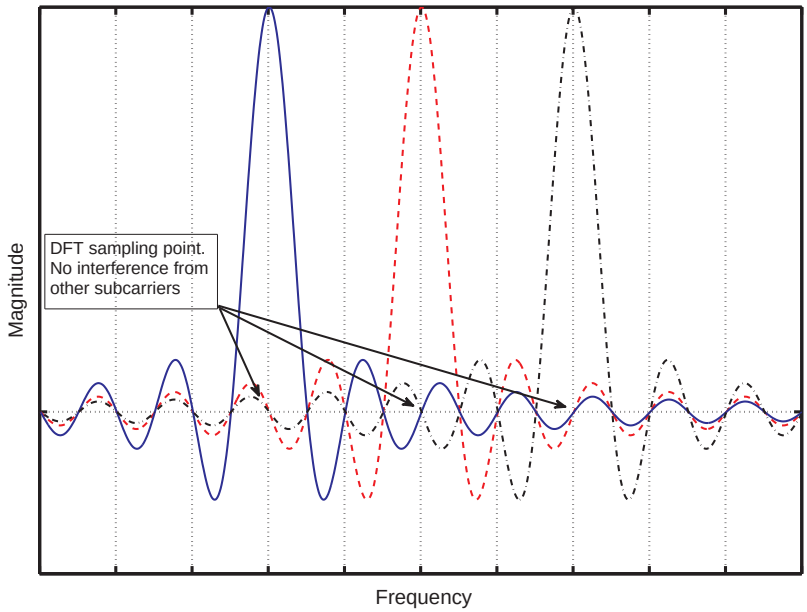

(a) OFDM signal without phase noise

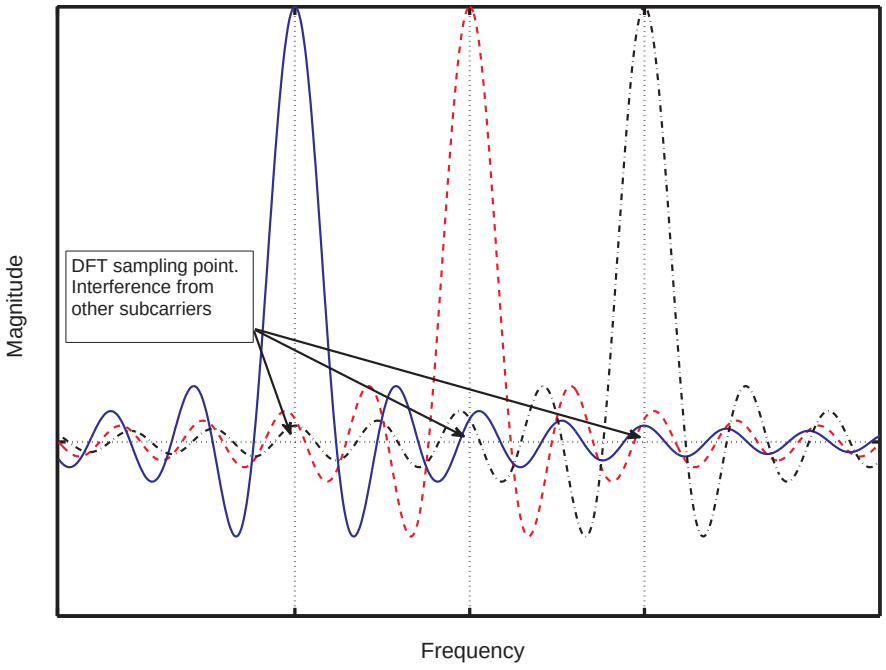

(b) OFDM signal with phase noise

Figure 3.2: Comparison between OFDM frequency spectrum with and without phase noise.

The expression for δ_{i-j} was obtained by making use of the Fourier transform property that convolution in the frequency domain is equivalent to multiplication in time domain. Using

(3.17), (3.16) can be closely approximated as

$$r_j = H_j \delta_0 s_j + H_j \sum_{k=0, k\neq j}^{N_c-1} \delta_{k-j} s_k + n_j. \tag{3.19}$$

3.3 Signal to Interference-Plus-Noise-Ratio

In order to evaluate the SINR per subcarrier, we assume first that the input symbols $\{s_j\}_{j=0}^{N_c-1}$ are independent of each other. The noise n_j is also assumed independent of the input symbols as well as of the phase noise. The channel coherence time [42] is typically larger compared to the OFDM symbol length, and thus, H_j can be assumed constant over the symbol length. From (3.19), taking the expectation of $|r_j|^2$ conditioned on fixed δ_k and H_j we have

$$E\Big[|r_j|^2\Big|H_j, \delta_k\Big] = |H_j|^2|\delta_0|^2\sigma_s^2 + |H_j|^2 \sum_{k=0, k\neq j}^{N_c-1} |\delta_{k-j}|^2\sigma_s^2 + \sigma_n^2, \tag{3.20}$$

where $\sigma_s^2 = E\Big[|s_j|^2\Big], \sigma_n^2 = E\Big[|n_j|^2\Big]$ are the respective signal and noise powers. The SINR for the jth subcarrier can then be expressed as

$$\gamma_j = \frac{|H_j|^2|\delta_0|^2\sigma_s^2}{\Big(|H_j|^2 \sum_{k=0,k\neq j}^{N_c-1} |\delta_{k-j}|^2\Big)\sigma_s^2 + \sigma_n^2}. \tag{3.21}$$

From the definition of δ_k in (3.18), by the Parseval's theorem we have

$$\frac{1}{N_c}\sum_{k\ =0}^{Nc-1} |\delta_k|^2 = \sum_{k=0}^{Nc-1} |\frac{e^{j(\theta_T[n]+\theta_R[n])}}{N_c}|^2, \tag{3.22a}$$

$$\sum_{k=0}^{Nc-1} |\delta_k|^2 = 1\,,\ \text{and, hence,}\quad |\delta_0|^2 = 1 - \sum_{k=1}^{Nc-1} |\delta_k|^2. \tag{3.22b}$$

Using (3.22b) in (3.21), we have the final expression for the SINR as

$$\gamma_j = \frac{1-y}{y + \frac{\sigma_n^2}{\sigma_s^2 g_j}}, \tag{3.23}$$

where

$$y = \sum_{k=1}^{N_c-1} |\delta_k|^2,\ g_j = |H_j|^2. \tag{3.24}$$

In arriving at (3.23), we have used the fact that, irrespective of index j, the summation in the denominator of (3.21) would be composed of the same $\{\delta_k\}_{k=1}^{N_c-1}$.

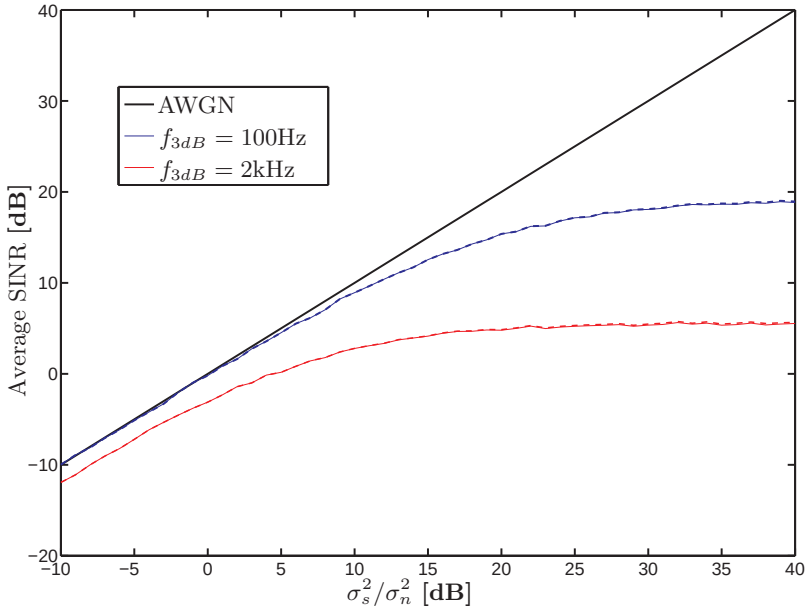

Figure 3.3: Comparison between average SINR γ_j and the SINR corresponding to (3.16). The dashed lines represent γ_j. OFDM system parameters are chosen as follows: Bandwidth is 20MHz, $N_c = 1024$ and $f_{sub} = 19.531$kHz. The 3dB bandwidth of the oscillator PSD is denoted by f_{3dB}. Channel is Rayleigh fading with five taps and coherence bandwidth is 300kHz with exponential power-delay profile.

We now spare a moment in giving a meaningful name to y. From the definition of y in (3.24), we see that it is always composed of unwanted subcarriers that cause interference to the desired subcarrier. It can be looked as the total power of the interfering subcarriers. It is, hence, fitting to call y as the ICI power. From (3.22b), we see that the power of the CPE and ICI power always add up to one, and hence can be looked as being complementary to one and another.

Using simulations, we show that the system model in (3.19) is a good approximation to (3.16). The comparison between these system models is done in terms of the average SINR. Figure 3.3 shows the average SINR plots corresponding to (3.23) compared with the exact SINR one would obtain using (3.16). Clearly, Fig. 3.3 justifies the use of the SINR as in (3.23) and hence of the signal model in (3.19).

Denoting the respective random variables of the realizations y and g_j by Y and G_j, (3.23) shows how the SINR depends on the phase noise process (at the transmitter and receiver) and the channel. Because Y and G_j can be assumed independent of each other, the average SINR (or average of any function of the SINR) is obtained by sequentially averaging over the PDFs of Y and G_j. Assuming a Rayleigh fading channel, our aim now is to determine the PDF of Y, which we derive in Chapter 4, before which, we digress in the following

section to discuss the Wiener phase noise model.

3.4 Wiener Phase Noise Process

It is shown in [11] that, for autonomous oscillators, as $t \to \infty$, the phase noise $\theta(t)$ becomes asymptotically a Gaussian process with variance $\sigma^2 = ct$ that linearly increases with time, c being the rate of the variance whose value depends on the kind of oscillator used. We can describe such a process as being a Wiener process or Brownian motion.

Definition A process is said to be Wiener if it satisfies the following

- $\theta(0) = 0$.
- $\theta(t_2) - \theta(t_1) \sim \mathcal{N}(0, c(t_2 - t_1))$ for all $t_2 \geq t_1 \geq 0$.
- $\theta(t_1), \theta(t_2) - \theta(t_1), \theta(t_3) - \theta(t_2) \ldots \theta(t_n) - \theta(t_{n-1})$ are all independent increments for all $t_n \geq t_{n-1} \geq t_{n-2} \ldots t_2 \geq t_1$.

Here $X \sim \mathcal{N}(\mu, \sigma^2)$ denotes the random variable X follows a Gaussian distribution with mean μ and variance σ^2. A discrete Wiener process $\theta(nT_s)$ is obtained by sampling its continuous-time counterpart $\theta(t)$. From the third property of a Wiener process, we have the following

$$\theta[n] = \sum_{i=0}^{n} \varepsilon(i), \tag{3.25}$$

where, by definition of the Wiener phase noise process, $\theta[0] = \varepsilon(0) = 0$ and $\varepsilon(i) = \theta[i] - \theta[i-1]$ are the independent increments drawn from a zero mean Gaussian distribution with variance [52] given below as

$$\sigma^2 = cT_s = \frac{c}{f_{sub}N_c} = \frac{4\pi f_{3dB}}{f_{sub}N_c}. \tag{3.26}$$

Another means of characterizing the phase noise process $\theta(t)$ is by looking at the PSD of the oscillator. Although from the definition of the Wiener process, we see that the process is non-stationary with variance increasing with time, suggesting a non-stable system, however, the oscillator process $a(t) = e^{j(2\pi f_c t + \theta(t))}$ is a stationary process and hence a stable one [52]. This is easily verified by taking the auto-correlation function of $a(t)$ i.e.

$$R_a(t, t+\tau) = E\left[a^*(t)a(t+\tau)\right] = e^{-\frac{1}{2}c|\tau|}e^{j2\pi f_c \tau}, \tag{3.27}$$

where we made use of the second property of Wiener process and that for $X \sim \mathcal{N}(0, \sigma^2)$, we have

$$E\left[e^{jX}\right] = e^{-\frac{1}{2}E[X^2]}. \tag{3.28}$$

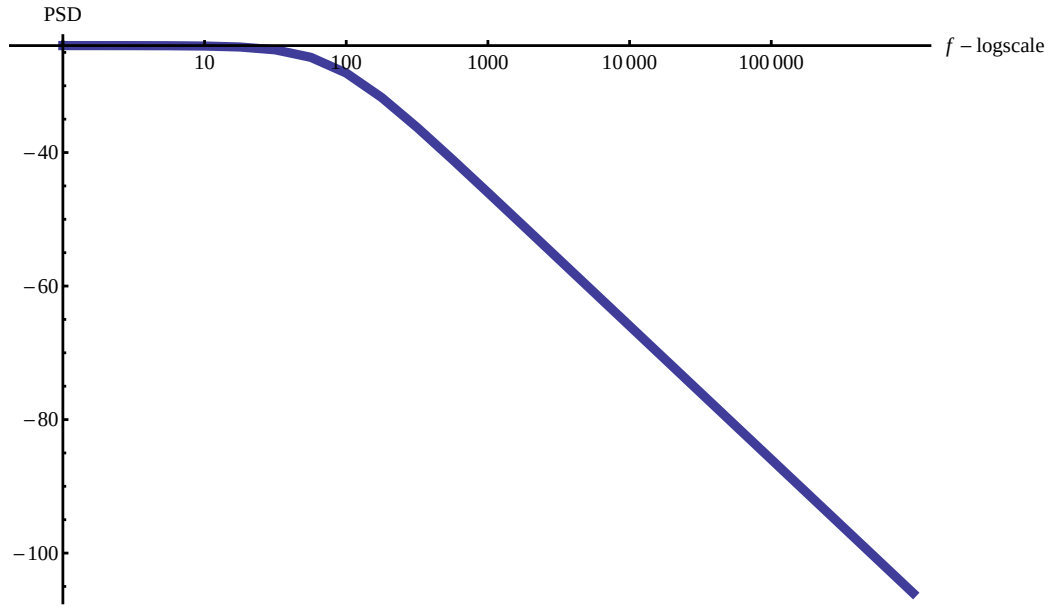

Figure 3.4: PSD of oscillator impaired by Wiener phase noise. The 3dB bandwidth is chosen as 80Hz.

Clearly, from (3.27), we see no time dependence of the autocorrelation function. The PSD of oscillator is obtained by taking the fourier transform of (3.27) to obtain

$$S(\omega) = \frac{c/2}{(\Delta\omega)^2 + (c/2)^2}, \tag{3.29}$$

where $\Delta\omega = 2(\pi f - \pi f_c)$. Clearly, (3.29) shows the spreading of the spectrum in comparison to an ideal oscillator. The slope of the PSD can be used as measure of the spread. For reasonably small 3dB bandwidths of PSD, we can approximate (3.29) as

$$S(\omega) = \frac{c/2}{(\Delta\omega)^2}, \tag{3.30}$$

from which we get a -20dB/decade slope from the 3dB bandwidth onwards. Figure (3.4) shows a typical oscillator single side band PSD plot for the Wiener phase noise. It is obtained by evaluating (3.29) only for positive $\Delta\omega$ and multiplying the result by a factor of two. With this phase noise model in mind, we now proceed, in the next chapter, to determine the distribution of the ICI power of (3.24).

Chapter 4

Probability Density Function of the ICI Power

In the previous chapter, we showed the dependence of the instantaneous SINR, in (3.23), on the phase noise process through the random variable Y defined in (3.24). We call Y as the ICI power from its very definition. The knowledge of the distribution of the ICI power provides means to evaluate statistical measures such as average SINR, average capacity etc.

In this chapter, we show that, for the Wiener phase noise process, the ICI power can be expressed as a sum of gamma random variables using a Taylor series approximation. The validity of the approximation requires that the ratio of the subcarrier spacing and the 3dB bandwidth of the oscillator PSD to be large. In Chapter 6, we quantify this ratio over which the approximation holds and is true for most practical oscillators and standards. With this meaningful characterization of the ICI power, we next derive the PDF of a sum of gamma variables. A similar result was derived in [2, Eq. (5)]. The PDF, however, is applicable only when square root of the normalized covariance matrix of the gamma variables is full-rank. We generalize the result for the rank-deficient case and apply it to Y. Finally, for the Taylor series approximation of Y, we present the structure of the normalized covariance matrix of the gamma variables. This is necessary as the parameters of the PDF are the eigenvalues which are obtained from this matrix.

4.1 Taylor Series Approximation of the ICI Power

Proposition 4.1.1 *As long as the accumulated variance of the Wiener phase noise process over one OFDM symbol is sufficiently small, i.e.,* $\sigma^2_{max} = (N_c - 1)\sigma^2$*, y is a sum of* $N =$

$\frac{N_c(N_c-1)}{2}$ *correlated gamma variables as follows*

$$y = \sum_{k=1}^{N_c-1} |\delta_k|^2 \approx \sum_{l=1}^{N_c-1} \sum_{i=1}^{N_c-l} Z_{il}, \tag{4.1}$$

where Z_{il} *follows a gamma distribution with parameters* $\alpha = 1/2$ *and* $\beta_l = \frac{2\sigma^2 l}{N_c^2}$ *(*$Z_{il} \sim \mathcal{G}(1/2, \frac{2\sigma^2 l}{N_c^2})$*) and is given as*

$$Z_{il} = \frac{1}{2}\beta_l \left(\frac{\sum_{j=0}^{l-1} \varepsilon(i + mN_c + j)}{\sqrt{l}\sigma} \right)^2. \tag{4.2}$$

Proof: From (3.24), the expression for y is given as $y = \sum_{k=1}^{N_c-1} |\delta_k|^2$, where δ_k is given in (3.18). Assuming independent transmit and receive phase noise processes, we can say that the combined process $\theta[n] = \theta_T[n] + \theta_R[n]$ in (3.18) is still a discrete Wiener process. Using (3.25) in (3.18), we can write the real and imaginary parts of δ_k as

$$\mathrm{Re}\{\delta_k\} = \frac{1}{N_c} \left[\sum_{l=0}^{N_c-1} \cos\left(\sum_{j=0}^{mN_c+l} \varepsilon(j) - \frac{2\pi k(mN_c + l)}{N_c} \right) \right], \tag{4.3a}$$

$$\mathrm{Im}\{\delta_k\} = \frac{1}{N_c} \left[\sum_{l=0}^{N_c-1} \sin\left(\sum_{j=0}^{mN_c+l} \varepsilon(j) - \frac{2\pi k(mN_c + l)}{N_c} \right) \right]. \tag{4.3b}$$

We denote the arguments of the cosine and sine functions in the above expression as

$$A_l = \sum_{j=0}^{mN_c+l} \varepsilon(j) - \frac{2\pi k(mN_c + l)}{N_c}. \tag{4.4}$$

Squaring (4.3a) and (4.3b) and applying the following binomial expansion,

$$\left(\sum_{i=0}^{N-1} x_i \right)^2 = \sum_{l=0}^{N-1} x_l^2 + 2 \sum_{l=1}^{N-1} \sum_{i=1}^{N-l} x_{i+l-1} x_{l-1}, \tag{4.5}$$

to the real and imaginary parts and then summing, gives the squared magnitude of $|\delta_k|^2$ as follows

$$\begin{aligned} |\delta_k|^2 &= \frac{1}{N_c^2} \left[\sum_{l=0}^{N_c-1} \Big(\cos^2(A_l) + \sin^2(A_l) \Big) + 2 \sum_{l=1}^{N_c-1} \sum_{i=1}^{N_c-l} \cos(A_{i+l-1}) \cos(A_{l-1}) \right. \\ &\qquad \left. + \sin(A_{i+l-1}) \sin(A_{l-1}) \right], \\ &= \frac{1}{N_c^2} \left[N_c + 2 \sum_{l=1}^{N_c-1} \sum_{i=1}^{N_c-l} \cos(A_{i+l-1} - A_{l-1}) \right], \end{aligned} \tag{4.6}$$

where the trigonometric identity $\cos(A)\cos(B)+\sin(A)\sin(B)=\cos(A-B)$ is used. Using (4.4) in (4.6) and re-arranging the terms, we finally get

$$|\delta_k|^2 = \frac{1}{N_c^2}\left[N_c + 2\sum_{l=1}^{N_c-1}\sum_{i=1}^{N_c-l}\cos\left(\sum_{j=0}^{l-1}\varepsilon(i+mN_c+j) - \frac{2\pi kl}{N_c}\right)\right]. \tag{4.7}$$

The arguments of the cosine functions in (4.7) are Gaussian random variables with mean $-\frac{2\pi kl}{N_c}$ in which $l = 1, 2, \ldots, N_c - 1$. For $l = 1$, the arguments have variance σ^2. For $l = 2$, the variance is $2\sigma^2$ and so on till $l = N_c - 1$ with variance equal to $(N_c - 1)\sigma^2$. If the largest variance $\sigma^2_{max} = (N_c - 1)\sigma^2$ is small enough, we can use a Taylor series approximation around the point $-\frac{2\pi kl}{N_c}$ and restrict the approximation up to to the second order polynomial. Doing this for the cosine term in above equation we have

$$\begin{aligned}|\delta_k|^2 \approx \frac{1}{N_c^2}\Bigg[N_c + 2\sum_{l=1}^{N_c-1}\sum_{i=1}^{N_c-l}\cos\left(-\frac{2\pi kl}{N_c}\right) - \sum_{l=1}^{N_c-1}\sum_{i=1}^{N_c-l}\sin\left(-\frac{2\pi kl}{N_c}\right)\left(\sum_{j=0}^{l-1}\varepsilon(i+mN_c+j)\right)\\ - \sum_{l=1}^{N_c-1}\sum_{i=1}^{N_c-l}\cos\left(-\frac{2\pi kl}{N_c}\right)\left(\sum_{j=0}^{l-1}\varepsilon(i+mN_c+j)\right)^2\Bigg].\end{aligned} \tag{4.8}$$

Now, summing the above equation over k, i.e., the sum $y = \sum_{k=1}^{N_c-1}|\delta_k|^2$ reduces to (4.1) after using the fact that $\sum_{k=1}^{N_c-1}\cos(\frac{-2\pi kl}{N_c}) = -1$ and $\sum_{k=1}^{N_c-1}\sin(\frac{-2\pi kl}{N_c}) = 0$.

Remark 4.1.2 *Through the definition of σ^2 in (3.26), we can write σ^2_{max} as*

$$\sigma^2_{max} = (N_c-1)\sigma^2 = \frac{(N_c-1)4\pi f_{3dB}}{f_{sub}N_c} \approx \frac{4\pi f_{3dB}}{f_{sub}} \;\; \textit{with} \;\; N_c \gg 1. \tag{4.9}$$

From (4.9), we see that f_{sub} and f_{3dB} determine the accuracy of the approximation in (4.1). Now, for each l in (4.1), the gamma variables $\{Z_{il}\}_{i=1}^{N_c-l}$ have the same parameters of $\alpha = \frac{1}{2}$ and $\beta_l = \frac{2\sigma^2 l}{N_c^2}$.

In the following section, we derive the PDF of a sum of N gamma random variables with normalized covariance matrix $\mathbf{M_z}$. In [2, Eq. (5)], the PDF was derived using the moment generating function (MGF) approach of [25]. This, however, is not applicable if the element-wise square-root of $\mathbf{M_z}$ (i.e., $(\mathbf{M_x})_{ij} = \sqrt{(\mathbf{M_z})_{ij}},\ i,j = 1,2,\ldots,N$) is rank-deficient which is the case for the gamma variables Z_{il} in (4.2). Therefore, we generalize next the result of [2, Eq. (5)] for the rank-deficient case and apply this to Y in (4.1).

4.2 PDF of Sum of Gamma Variables

Let $\{Z_n\}_{n=1}^N$ be a set of N correlated gamma variates with normalized covariance matrix $\mathbf{M_z}$, i.e., $Z_n \sim \mathcal{G}(\alpha, \beta_n)$. Each Z_n is constructed from a set of 2α i.i.d. N-dimensional Gaussian random vectors, $\mathbf{x}_i$, $i = 1, \ldots, 2\alpha$, each with the same covariance matrix $\mathbf{M_x}$ [25], i.e.,

$$Z_n = \frac{1}{2}\beta_n \sum_{i=1}^{2\alpha} x_{ni}^2, n = 1, \ldots, N, \tag{4.10}$$

where $(\mathbf{M_x})_{ij} = \sqrt{(\mathbf{M_z})_{ij}},\ i, j = 1, 2, \ldots, N$ [21]. The components of $\mathbf{x}_i = [x_{1i}, x_{2i} \ldots x_{Ni}]^{\mathrm{T}}$ are Gaussian random variables with zero mean and unit variance.

The PDF derived in [2, Eq. (5)] is obtained by first constructing the moment generating function (MGF) of $\sum_{n=1}^N Z_n$ which assumes that $\mathbf{M_x}$ is full-rank. Comparing (4.2) with (4.10), we have $2\alpha = 1$, and thus only one Gaussian random vector is used to generate Z_{il} $\forall\ l = 1, 2 \ldots, N_c - 1, i = 1, 2 \ldots, N_c - l$. The structure of this Gaussian vector from (4.1) and (4.2) can be obtained as follows

$$\mathbf{x} = \left[\mathbf{x}_1^{\mathrm{T}}\ \mathbf{x}_2^{\mathrm{T}}\ \ldots\ \mathbf{x}_{(N_c-1)}^{\mathrm{T}}\right]^{\mathrm{T}}, \tag{4.11}$$

where $\mathbf{x}_l$ is an $(N_c - l) \times 1$ column vector with elements

$$(\mathbf{x}_l)_i = \sum_{j=0}^{l-1} \left(\frac{\varepsilon(i + mN_c + j)}{\sqrt{l\sigma^2}}\right),\ i = 1, 2 \ldots, N_c - l. \tag{4.12}$$

From (4.11) and (4.12), the covariance matrix $\mathbf{M_x}$ of $\mathbf{x}$ will be rank-deficient with rank $N_c - 1$. This is because the elements of $\mathbf{x}$ are constructed from only $N_c - 1$ independent Gaussian random variables. With this background, we present next the PDF of a sum of gamma random variables for any rank of $\mathbf{M_x}$.

Theorem 4.2.1 *Let $\{Z_n\}_{n=1}^N$ be a set of N correlated gamma variates ($Z_n \sim \mathcal{G}(\alpha, \beta_n)$) with normalized covariance matrix $\mathbf{M_z}$ of any rank $R \leq N$. Then, the PDF of $Y = \sum_{n=1}^N Z_n$ is given as*

$$p_Y(y) = \prod_{n=1}^{R} \left(\frac{\lambda_1}{\lambda_n}\right)^{\alpha} \sum_{k=0}^{\infty} \frac{\zeta_k y^{R\alpha+k-1} e^{\frac{-y}{\lambda_1}}}{\lambda_1^{R\alpha+k}\Gamma(R\alpha + k)}, \tag{4.13}$$

where $\{\lambda_n\}_{n=1}^R$ are the ordered eigenvalues of the matrix $\mathbf{PBP}^{\mathrm{T}}\mathbf{\Delta}$ with λ_1 being the minimum. The $\mathbf{P}$ and $\mathbf{\Delta}$ matrices are obtained from eigenvalue decomposition of $\mathbf{M_x}$ which is related to $\mathbf{M_z}$ as

$$(\mathbf{M_x})_{ij} = \sqrt{(\mathbf{M_z})_{ij}},\ \ i, j = 1, 2, \ldots, N. \tag{4.14}$$

$$\mathbf{M_x} = \mathbf{C\Sigma C}^{\mathrm{T}}, \quad \mathbf{\Sigma} = \begin{bmatrix} \mathbf{\Delta}_{R\times R} & \mathbf{0} \\ \mathbf{0} & \mathbf{0} \end{bmatrix}, \quad \mathbf{C} = \begin{bmatrix} \mathbf{c}_1 & \mathbf{c}_2 & \dots & \mathbf{c}_R & \mathbf{\Omega}_1 & \mathbf{\Omega}_2 & \dots & \mathbf{\Omega}_{N-R} \end{bmatrix}. \tag{4.15}$$

$$\mathbf{P} = [\mathbf{c}_1 \ \mathbf{c}_2 \ \dots \ \mathbf{c}_R]^{\mathrm{T}}, \tag{4.16a}$$
$$\mathbf{B} = \mathrm{diag}(\beta_1 \ \beta_2 \ \dots \ \beta_N). \tag{4.16b}$$

The weights $\zeta_k, k = 0, 1, 2, \dots,$ are given as

$$\zeta_0 = 1, \quad \zeta_{k+1} = \frac{\alpha}{k+1} \sum_{i=1}^{k+1} \Big(\sum_{j=1}^{R} (1 - \frac{\lambda_1}{\lambda_j})^i \Big) \zeta_{k+1-i}. \tag{4.17}$$

Proof: Let $\mathbf{x}$ be an N-dimensional Gaussian random vector with covariance matrix $\mathbf{M_x}$ of rank $R \leq N$. The multi-variate PDF of $\mathbf{x}$ is given as [30, Chapter 3]

$$p_X(\mathbf{x}) = \frac{1}{(2\pi)^{\frac{R}{2}} |\mathbf{\Delta}|^{\frac{1}{2}}} \exp(\frac{-1}{2} \mathbf{x}^{\mathrm{T}} \mathbf{M}_{\mathbf{x}}^{+} \mathbf{x}) \prod_{k=1}^{N-R} \delta(\mathbf{x}^{\mathrm{T}} \mathbf{\Omega}_k), \tag{4.18}$$

where $\mathbf{M}_{\mathbf{x}}^{+}$ is the pseudoinverse of $\mathbf{M_x}$. The Dirac delta function is denoted by $\delta(\cdot)$ and $|\mathbf{\Delta}|$ is the product of the nonzero eigenvalues of $\mathbf{M_x}$. The PDF defined above is quite intuitive: It clearly shows that PDF of the random vector $\mathbf{x}$ is defined only in the R-dimensional subspace spanned by the eigenvectors $\{\mathbf{c}_k\}_{k=1}^{R}$ and is zero in the $(N-R)$-dimensional subspace spanned by the vectors $\{\mathbf{\Omega}_k\}_{k=1}^{N-R}$. This should be expected as a random vector $\mathbf{x}$ having a covariance matrix of rank $R \leq N$ will always lie in an R-dimensional subspace [65, Appendix C].

The MGF of Y is given by

$$E\left[e^{sY}\right] = \int_{-\infty}^{\infty} e^{sY} p(Y) dY. \tag{4.19}$$

Using (4.10), we can write $Y = \sum_{n=1}^{N} Z_n$ as follows

$$Y = \frac{1}{2} \sum_{n=1}^{N} \sum_{i=1}^{2\alpha} \beta_n x_{ni}^2 = \frac{1}{2} \sum_{i=1}^{2\alpha} \mathbf{x}_i^{\mathrm{T}} \mathbf{B} \mathbf{x}_i, \tag{4.20}$$

where $\mathbf{B}$ is defined in (4.16b). Using (4.20) in (4.19) we have

$$E\left[e^{sY}\right] = \int_{-\infty}^{\infty} \dots \int_{-\infty}^{\infty} e^{s\frac{1}{2}\sum_{i=1}^{2\alpha} \mathbf{x}_i^{\mathrm{T}} \mathbf{B} \mathbf{x}_i} p_{X_1}(x_1) dx_1 \dots p_{X_{2\alpha}}(x_{2\alpha}) dx_{2\alpha}, \tag{4.21}$$

where the fact that, joint PDF of mutually independent $\{X_i\}_{i=1}^{2\alpha}$ is a product of their

respective PDFs was used. Using (4.18) in the above equation, the MGF of Y becomes

$$\begin{aligned} M_Y(s) &= \prod_{i=1}^{2\alpha} \int_{-\infty}^{\infty} \frac{e^{\frac{1}{2}s\mathbf{x}_i^{\mathrm{T}}\mathbf{B}\mathbf{x}_i} e^{-\frac{1}{2}(\mathbf{x}_i^{\mathrm{T}}\mathbf{M}_{\mathbf{x}}^{+}\mathbf{x}_i)} \prod_{k=1}^{N-R} \delta(\mathbf{x}_i^{\mathrm{T}}\boldsymbol{\Omega}_k)}{(2\pi)^{\frac{R}{2}}|\boldsymbol{\Delta}|^{\frac{1}{2}}} \mathbf{d}\mathbf{x}_i, \\ &= \left[\int_{-\infty}^{\infty} \frac{e^{-\frac{1}{2}\mathbf{x}^{\mathrm{T}}[\mathbf{M}_{\mathbf{x}}^{+} - s\mathbf{B}]\mathbf{x}} \prod_{k=1}^{N-R} \delta(\mathbf{x}^{\mathrm{T}}\boldsymbol{\Omega}_k)\mathbf{d}\mathbf{x}}{(2\pi)^{\frac{R}{2}}|\boldsymbol{\Delta}|^{\frac{1}{2}}} \right]^{2\alpha}. \end{aligned} \tag{4.22}$$

The integrand in (4.22) will be non-zero only for vectors $\mathbf{x}$ in the R-dimensional subspace and zero elsewhere. This implicitly means we perform the integration in an R-dimensional subspace. Thus, in order to evaluate the above integral, we could equivalently do a transformation $\mathbf{y} = \mathbf{P}\mathbf{x}$ from the N-dimensional space to an R-dimensional space, such that

- Null space of $\mathbf{P}$ is the $(N-R)$-dimensional subspace spanned by the vectors $\{\boldsymbol{\Omega}_k\}_{k=1}^{N-R}$, i.e., Null($\mathbf{P}$) = span $\left\{\boldsymbol{\Omega}_1\boldsymbol{\Omega}_2 \ldots \boldsymbol{\Omega}_{N-R}\right\}$.
- $\mathbf{P}$ is an isometry w.r.t R-dimensional subspace of $\mathbf{x}$ and R-dimensional space of $\mathbf{y}$.

The second condition ensures the Jacobian to be unity. Such a transformation $\mathbf{P}$ is defined in (4.16a). Thus, expressing $\mathbf{x} = \mathbf{P}^{+}\mathbf{y} = \mathbf{P}^{\mathrm{T}}\mathbf{y}$ and inserting this into (4.22) gives

$$\begin{aligned} M_Y(s) &= \left[\int_{-\infty}^{\infty} \frac{e^{-\frac{1}{2}(\mathbf{P}^{\mathrm{T}}\mathbf{y})^{\mathrm{T}}[\mathbf{M}_{\mathbf{x}}^{+} - s\mathbf{B}]\mathbf{P}^{\mathrm{T}}\mathbf{y}} \prod_{k=1}^{N-R} \delta((\mathbf{P}^{\mathrm{T}}\mathbf{y})^{\mathrm{T}}\boldsymbol{\Omega}_k)\mathbf{d}\mathbf{y}}{(2\pi)^{\frac{R}{2}}|\boldsymbol{\Delta}|^{\frac{1}{2}}} \right]^{2\alpha}, \\ &= \left[\int_{-\infty}^{\infty} \frac{e^{-\frac{1}{2}\mathbf{y}^{\mathrm{T}}[(\mathbf{P}\mathbf{M}_{\mathbf{x}}\mathbf{P}^{\mathrm{T}})^{+} - s\mathbf{P}\mathbf{B}\mathbf{P}^{\mathrm{T}}]\mathbf{y}}\mathbf{d}\mathbf{y}}{(2\pi)^{\frac{R}{2}}|\boldsymbol{\Delta}|^{\frac{1}{2}}} \right]^{2\alpha}, \\ &= \left[\frac{\left|(\mathbf{P}\mathbf{M}_{\mathbf{x}}\mathbf{P}^{\mathrm{T}})^{+} - s\mathbf{P}\mathbf{B}\mathbf{P}^{\mathrm{T}}\right|^{-\frac{1}{2}}}{|\boldsymbol{\Delta}|^{\frac{1}{2}}} \right]^{2\alpha}. \end{aligned} \tag{4.23}$$

Now using $(\mathbf{P}\mathbf{M}_{\mathbf{x}}\mathbf{P}^{\mathrm{T}})^{+} = \boldsymbol{\Delta}^{+} = \boldsymbol{\Delta}^{-1}$ in (4.23), the MGF of Y becomes

$$\begin{aligned} M_Y(s) &= \left[\frac{\left|\boldsymbol{\Delta}^{-1} - s\mathbf{P}\mathbf{B}\mathbf{P}^{\mathrm{T}}\right|^{-\frac{1}{2}}}{|\boldsymbol{\Delta}|^{\frac{1}{2}}} \right]^{2\alpha} = \left|\mathbf{I} - s\mathbf{P}\mathbf{B}\mathbf{P}^{\mathrm{T}}\boldsymbol{\Delta}\right|^{-\alpha}, \\ &= \prod_{n=1}^{R} (1 - s\lambda_n)^{-\alpha}, \end{aligned} \tag{4.24}$$

where the last step is obtained as used in [23] and λ_n are the R eigenvalues of the matrix $\mathbf{P}\mathbf{B}\mathbf{P}^{\mathrm{T}}\boldsymbol{\Delta}$. Using the Moschopoulos technique [34] of inverting the MGF of Y, we obtain the PDF in (4.13).

Remark 4.2.2 *In the full-rank case, $R = N$, $\mathbf{P} = \mathbf{C}^{\mathrm{T}}$, $\boldsymbol{\Delta} = \boldsymbol{\Sigma}$ and $\mathbf{P}\mathbf{B}\mathbf{P}^{\mathrm{T}}\boldsymbol{\Delta} = \mathbf{C}^{\mathrm{T}}\mathbf{B}\mathbf{M}_{\mathbf{x}}\mathbf{C}$.*

Since $\mathbf{C}$ *is a unitary matrix, the eigenvalues are the same as those of* $\mathbf{BM_x}$*, as was obtained in [2].*

4.3 PDF of ICI Power

The PDF of Y, defined in (4.1), is given by (4.13) with parameters

$$R = N_c - 1, \;\; \alpha = \frac{1}{2}, \;\; N = \frac{N_c(N_c-1)}{2}. \tag{4.25}$$

The eigenvalues are obtained from $\mathbf{PBP}^{\mathrm{T}}\mathbf{\Delta}$. The diagonal matrix $\mathbf{B}$ with elements β_n is given as

$$\mathbf{B} = \frac{2\sigma^2}{N_c^2}\,\mathrm{diag}\left(\mathbf{1}^{\mathrm{T}}_{(N_c-1)} \;\; 2\cdot\mathbf{1}^{\mathrm{T}}_{(N_c-2)} \;\; 3\cdot\mathbf{1}^{\mathrm{T}}_{(N_c-3)} \ldots (N_c-1)\cdot\mathbf{1}^{\mathrm{T}}_{1}\right), \tag{4.26}$$

where $\mathbf{1}_i$ denotes an i-dimensional column vector of ones. The respective $\mathbf{P}$ and $\mathbf{\Delta}$ matrix are obtained from $\mathbf{M_z}$, given in Appendix 4.4, through (4.14), (4.15) and (4.16a).

Remark 4.3.1 *From* (4.26)*, we see that the eigenvalues* $\{\lambda_n\}_{n=1}^{R}$ *are proportional to* σ^2 *and hence to* f_{3dB}/f_{sub} *from* (3.26)*.*

Figure 4.1 shows the PDF plots of Y for two different values of f_{3dB}. Clearly, Fig. 4.1a shows good correspondence between the simulated and analytical PDFs while in Fig. 4.1b one starts to see deviations. This is where the Taylor series approximation begins to break down. As mentioned in the previous subsection, the approximation holds as long as σ^2_{max} is small. From (4.9), we see that in order for (4.1) to hold, f_{sub} should be large compared to f_{3dB}. It is important to know at what value of σ^2_{max} does the approximation become intolerable. This tolerance limit can be specified depending upon the performance measure one wants to evaluate. That is, it is chosen to be that value of σ^2_{max} beyond which there is significant difference between the simulated and analytical performance measure. We specify this limit in terms of the average capacity which is elaborated more in Chapter 6.

In Fig. 4.2, the PDF of the ICI power is shown for differing values of the number of subcarriers N_c. Visible from the figure is the effect of increased ICI power with increasing N_c while keeping the bandwidth constant. This is because with increased N_c, the subcarrier spacing reduces, the interference from unwanted subcarriers increases and thereby, increased ICI power.

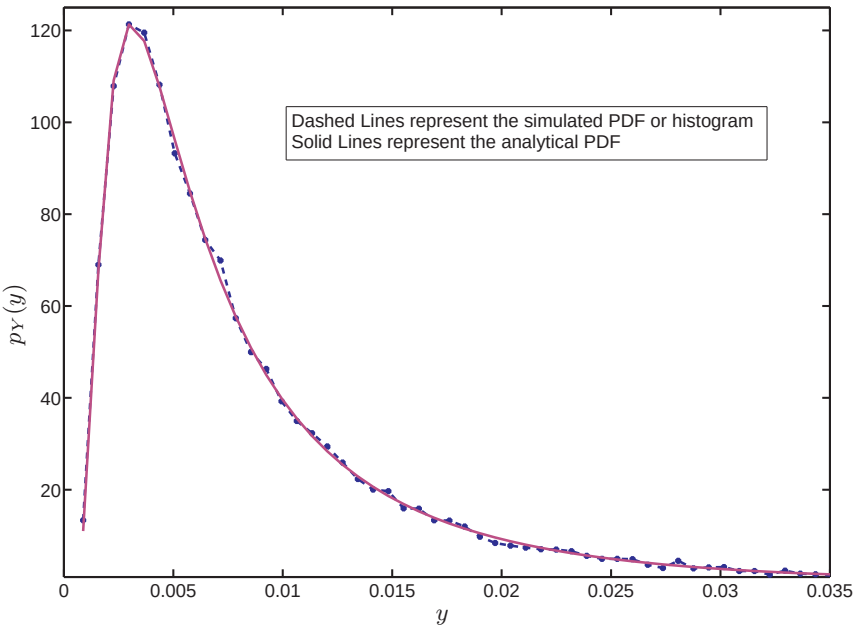

(a) $f_{3dB} = 80$Hz and hence $\sigma^2_{max} = 0.0515$

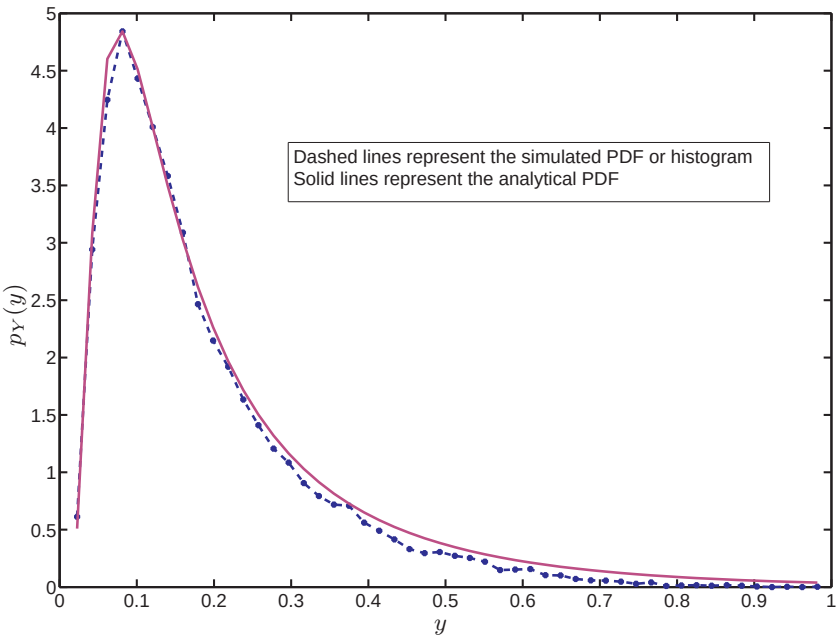

(b) $f_{3dB} = 2$kHz and hence $\sigma^2_{max} = 1.3228$

Figure 4.1: Comparison between analytical and simulated PDF of Y. Bandwidth is 625kHz, $N_c = 32$ and $f_{sub} = 19$kHz.

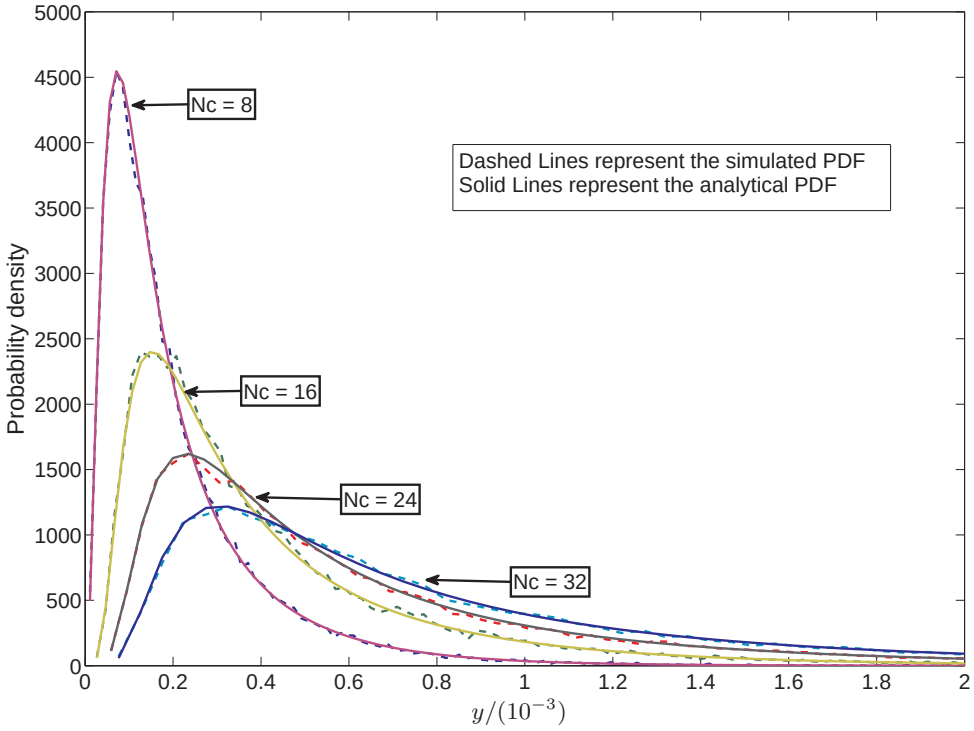

Figure 4.2: PDF of the ICI power for different values of N_c. The bandwidth of the OFDM system is 625kHz. The oscillator PSD 3dB bandwidth is 200Hz.

4.3.1 Mean of CPE and ICI Power

It is interesting and useful to know the second-order statistics of the CPE and ICI power. With the PDF of ICI power defined in (4.13) whose parameters are given by (4.25), we can evaluate the mean as follows

$$\begin{aligned}
\bar{Y} &= E[Y], \\
&= \int_0^\infty y p_Y(y) dy, \\
&= \int_0^\infty K \sum_{k=0}^{\infty} \frac{\zeta_k y^{R\alpha+k} e^{\frac{-y}{\lambda_1}}}{\lambda_1^{R\alpha+k}\Gamma(R\alpha+k)} dy, \\
&= K \sum_{k=0}^{\infty} \zeta_k \int_0^\infty \frac{y^{R\alpha+k} e^{\frac{-y}{\lambda_1}}}{\lambda_1^{R\alpha+k}\Gamma(R\alpha+k)} dy,
\end{aligned} \tag{4.27}$$

where $K = \prod_{n=1}^{R} \left(\frac{\lambda_1}{\lambda_n}\right)^{\alpha}$. The integral in the above equation is of the form [17, Eq (3.381.4)],

$$\int_0^{\infty} x^{v-1} e^{-\mu x} dx = \mu^{-v}\Gamma(v). \tag{4.28}$$

Applying (4.28) in (4.27) we get the final result for the mean as

$$\begin{aligned} \bar{Y} &= K \sum_{k=0}^{\infty} \zeta_k \frac{\left(\frac{1}{\lambda_1}\right)^{-(R\alpha+k+1)} \Gamma(R\alpha+k+1)}{\lambda_1^{R\alpha+k}\Gamma(R\alpha+k)}, \\ &= K \sum_{k=0}^{\infty} \zeta_k \frac{\lambda_1 \Gamma(R\alpha+k+1)}{\Gamma(R\alpha+k)}. \end{aligned} \tag{4.29}$$

Equation (4.29) can be used for evaluating the mean of the CPE power. The relation between the CPE power and its complement is given by (3.22b). Its mean can, thus, be evaluated as

$$\begin{aligned} \bar{Y}_{cpe} = E\left[|\delta_o|^2\right] &= E\left[1 - Y\right], \\ &= 1 - \bar{Y}, \\ &= 1 - K \sum_{k=0}^{\infty} \zeta_k \frac{\lambda_1 \Gamma(R\alpha+k+1)}{\Gamma(R\alpha+k)}. \end{aligned} \tag{4.30}$$

4.3.2 Variance of CPE and ICI Power

With PDF of Y at hand, the variance is evaluated as follows

$$\begin{aligned} \sigma_Y^2 &= E\left[(y-\bar{Y})^2\right] = E\left[y^2\right] - \bar{Y}^2, \\ &= \int_0^{\infty} y^2 p_Y(y) dy - \bar{Y}^2. \end{aligned} \tag{4.31}$$

Substituting the PDF of Y in (4.31) and making use of (4.28), the variance of the ICI power simplifies to

$$\sigma_Y^2 = K \sum_{k=0}^{\infty} \zeta_k \frac{\lambda_1^2 \Gamma(R\alpha+k+2)}{\Gamma(R\alpha+k)} - \bar{Y}^2. \tag{4.32}$$

From (3.22b), we see that CPE power is a simple linear translation of ICI power and hence its variance will be exactly the same as that of its complements. We, thus, have

$$\sigma_{Y_{cpe}}^2 = \sigma_Y^2. \tag{4.33}$$

Figure 4.3 shows the plots of the mean and variance of the CPE power and its complement for different values of 3dB bandwidth of the oscillator noise PSD. Clearly, we see that the

mean and variance of (4.29) and (4.32) deviate from their true values as the f_{3dB} increases. This is again attributed to the fact that the Taylor approximation does not hold any longer. However, from both the plots we see that error is of the order of 10^{-2} for f_{3dB} =1500 Hz. For such reasonable 3dB bandwidths, we show in Chapter 6 that this does not cause any significant difference between the analytical performance measures (derived in Chapter 5) and the simulations.

4.4 Structure of $\mathbf{M_z}$ for the Gamma Variables in (4.1)

To evaluate the PDF of Y given in (4.1), we need the eigenvalues which are obtained from the eigendecomposition of $\mathbf{M_x}$ which is related to $\mathbf{M_z}$ by (4.14). From the gamma variables defined in (4.1), we arrive at a block-matrix structure for $\mathbf{M_z}$ as follows

$$(\mathbf{M_z})_{ij} = \begin{cases} \mathbf{Z}_{ij} & j \geq i, i = 1, 2, \ldots, N_c - 1 \\ \mathbf{Z}_{ji}^{\mathrm{T}} & j \leq i, i = 1, 2, \ldots, N_c - 1 \end{cases}$$

where $\mathbf{Z}_{ij}$ is an $(N_c - i) \times (N_c - j)$ sub-matrix given as

$$\mathbf{Z}_{ij} = \text{Toeplitz}\Big[\mathbf{c}_{ij} \;\; \mathbf{r}_{ij}^{\mathrm{T}}\Big]\mathbf{J}_{ij}. \tag{4.34}$$

Above Toeplitz$[\mathbf{c}_{ij}\ \mathbf{r}_{ij}^{\mathrm{T}}]$ is the $(N_c-i)\times(N_c-i)$ Toeplitz matrix formed from the $(N_c-i)\times 1$ column vectors $\mathbf{c}_{ij}$ and $\mathbf{r}_{ij}$. The first element of $\mathbf{c}_{ij}$ corresponds to the diagonal. The second element corresponds to the first lower off diagonal and so on. It is given as

$$\mathbf{c}_{ij} = \Big[\frac{i}{j} \;\; \frac{i(i-1)^2}{j(i^2)}\mathbf{1}_{(j-i+1)}^{\mathrm{T}} \;\; \frac{i(i-2)^2}{j(i^2)} \;\; \frac{i(i-3)^2}{j(i^2)} \ldots \frac{i1}{j(i^2)} \;\; 0 \ldots 0\Big]^{\mathrm{T}}, \tag{4.35}$$

where $\mathbf{1_{(i-j+1)}}$ is $(j-i+1)\times 1$ column vector of ones. The vector $\mathbf{r}_{ij}$ is given as

$$\mathbf{r}_{ij} = \Big[\frac{i}{j} \;\; \frac{i(i-1)^2}{j(i^2)} \;\; \frac{i(i-2)^2}{j(i^2)} \ldots \frac{i1}{j(i^2)} \;\; 0 \ldots 0\Big]^{\mathrm{T}}, \tag{4.36}$$

where the first element of $\mathbf{r}_{ij}^{\mathrm{T}}$ corresponds to the diagonal, the second element to first upper off diagonal and so on. The $(N_c - i) \times (N_c - j)$ column selection matrix $\mathbf{J}_{ij}$ is given as

$$\mathbf{J}_{ij} = \begin{bmatrix} \mathbf{I}_{(N_c-j)\times(N_c-j)} \\ \mathbf{0}_{(j-i)\times(N_c-j)} \end{bmatrix}. \tag{4.37}$$

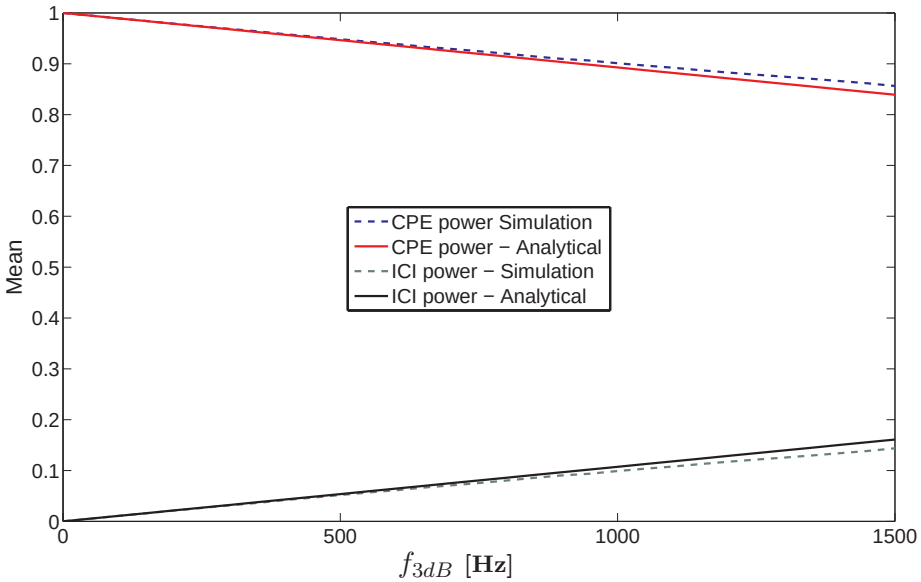

(a) Mean vs f_{3dB}

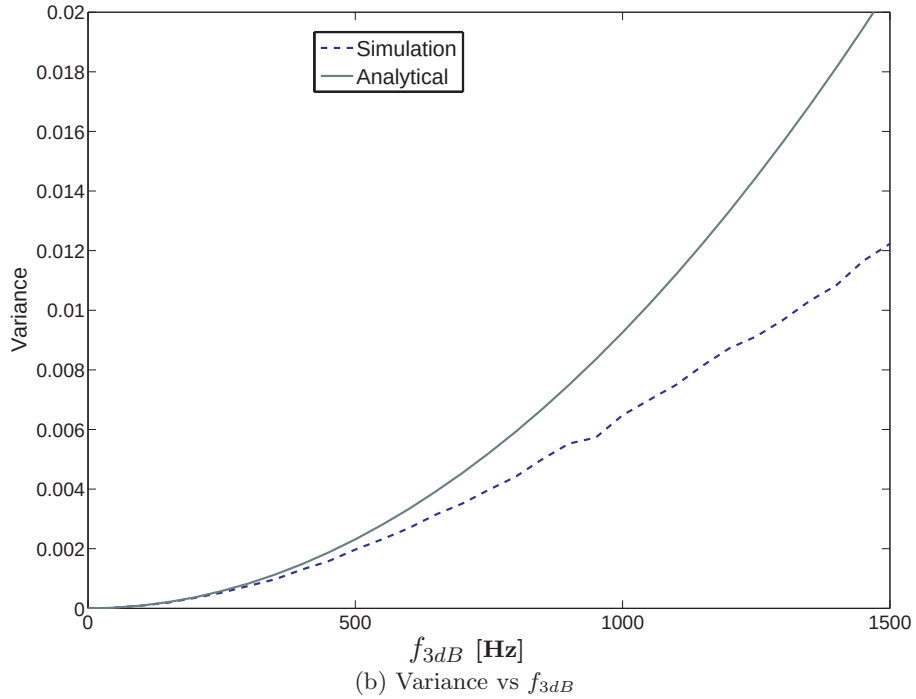

(b) Variance vs f_{3dB}

Figure 4.3: Comparison between analytical and simulated second order statistics of the CPE and ICI power. OFDM system parameters are as follows: Bandwidth is 625kHz, N_c = 32 and f_{sub} = 19kHz.

Chapter 5

Performance Measures

In this chapter, we derive closed-form expressions of average capacity, average SINR and outage capacity. From (3.19), we see how the desired data on the j^{th} subcarrier is corrupted by the CPE and ICI from other subcarriers along with noise. For a system model with the received signal comprising of the desired signal part plus the noise part and assuming independence between the two, with each drawn from the Gaussian distribution, the Shannon capacity is typically employed to evaluate the throughput.

With respect to (3.19), it is shown in [51] that the ICI cannot be regarded as a Gaussian random variable. However, we can come around this problem by using a PDF based approach as follows. The instantaneous SINR derived in (3.23) is conditioned on a fixed realization of the phase noise process and of the channel. Thus, if the input data $\{s_j\}_{j=0}^{N_c-1}$ are complex i.i.d. Gaussian RVs, then the ICI along with the receiver noise in (3.19) will also be complex Gaussian for this one realization. Thus, we may use the Shannon capacity for evaluating the throughput which will also be a random variable dependent upon different realizations of the phase noise process and the channel.

From (3.23), we see the dependence of the instantaneous SINR and, hence the Shannon capacity, on the random variables Y and G_j. The channel is described by G_j while Y, which denotes the ICI Power, characterizes the phase noise process. For the channel, we assume it is Rayleigh fading and the phase noise model is of the Wiener type. Having derived the PDF of Y for a Wiener process, we can, thus, evaluate the average SINR and average capacity.

5.1 Capacity

The instantaneous SINR is given by (3.23). It is derived for one realization of the phase noise process and of the channel. Consequently, the instantaneous Shannon capacity seen by the jth subcarrier is given by

$$\mathcal{C}_j = \log_2(1+\gamma_j), \tag{5.1}$$

where γ_j is given by (3.23) and repeated here

$$\gamma_j = \frac{1-y}{y+\frac{\sigma_n^2}{\sigma_s^2 g_j}}, \tag{5.2}$$

where

$$y = \sum_{k=1}^{N_c-1} |\delta_k|^2,\ g_j = |H_j|^2. \tag{5.3}$$

For ease of notation and without loss of generality, we drop the subscript j. In order to see the impact of only the phase noise on the capacity, we first fix G and average $\mathcal{C}$ over the PDF of Y. The result is then averaged over the distribution of G.

Before we proceed to derive the average capacity, we define the following definite integral and in the following subsection, we express it in terms of the exponential integral function.

$$I_{m-1} = \int_0^\infty \ln\Big(y+a\Big)\frac{y^{m-1}e^{-\mu y}}{\mu^{-m}\Gamma(m)}dy = e^{\mu a}\int_a^\infty \ln\Big(y\Big)\frac{(y-a)^{m-1}e^{-\mu y}}{\mu^{-m}\Gamma(m)}dy. \tag{5.4}$$

5.1.1 The Definite Integral $I_{(m-1)}$

Integrating (5.4) by parts gives

$$e^{-\mu a}\mu^{-m}\Gamma(m)I_{(m-1)} = (y-a)^{m-1}\int \ln(y)e^{-\mu y}dy\Big|_a^\infty - \int_a^\infty (m-1)(y-a)^{m-2}\int \ln(y)e^{-\mu y}dy. \tag{5.5}$$

The indefinite integral in the above equation is given by, after the application of integration by parts,

$$\begin{aligned}\int \ln(y)e^{-\mu y}dy &= \frac{\ln(y)e^{-\mu y}}{-\mu} + \frac{1}{\mu}\int \frac{e^{-\mu y}}{y}dy,\\ &= \frac{\ln(y)e^{-\mu y}}{-\mu} + \frac{1}{\mu}E_i(-\mu y),\end{aligned} \tag{5.6}$$

where $E_i(\cdot)$ is the exponential integral function [17, Eq. 8.211.1, 2.325.1] and is defined as

$$E_i(-x) = -\int_x^\infty \frac{e^{-t}}{t}dt = -\int_1^\infty \frac{e^{-xt}}{t}dt. \tag{5.7}$$

Substituting (5.6) into (5.5) and solving we have

$$\begin{aligned} e^{-\mu a}\mu^{-m}\Gamma(m)I_{(m-1)} &= \frac{1}{-\mu}(y-a)^{m-1}\ln(y)e^{-\mu y}\Big|_a^\infty + \frac{1}{\mu}(y-a)^{m-1}E_i(-\mu y)\Big|_a^\infty \\ &\quad + \frac{m-1}{\mu}\mu^{-(m-1)}\Gamma(m-1)I_{(m-2)} - \frac{m-1}{\mu}\int_a^\infty (y-a)^{m-2}E_i(-\mu y)dy, \\ &= \frac{m-1}{\mu}e^{-\mu a}\mu^{-(m-1)}\Gamma(m-1)I_{(m-2)} \\ &\quad - \frac{m-1}{\mu}\int_0^\infty y^{m-2}E_i(-\mu(y+a))dy. \end{aligned} \tag{5.8}$$

Now consider the definite integral in the above equation and after using (5.7), we have

$$\int_0^\infty y^{m-2}E_i(-\mu(y+a))dy = -\int_1^\infty \frac{e^{-\mu a t}}{t}\left(\int_0^\infty y^{m-2}\frac{e^{-\mu y t}}{t}dy\right)dt. \tag{5.9}$$

The inner integral in the above equation is solved using the result [17, Eq. 2.325.1]

$$\begin{aligned} \int_0^\infty y^{m-2}\frac{e^{(-\mu t)y}}{t}dy &= \left[e^{(-\mu t)y}\sum_{k=0}^{m-2}\frac{(-1)^k k!\binom{m-2}{k}}{(-\mu t)^(k+1)}y^{(m-2-k)}\right]_0^\infty, \\ &= -\frac{(-1)^{(m-2)}(m-2)!}{(-\mu t)^{(m-1)}}. \end{aligned} \tag{5.10}$$

Equation (5.9) is simplified to, after applying the above equation

$$\begin{aligned} \int_0^\infty y^{m-2}E_i(-\mu(y+a))dy &= \frac{(-1)^{(m-2)}(m-2)!}{(-\mu)^{(m-1)}}\int_1^\infty \frac{e^{-\mu a t}}{t^m}dt, \\ &= -\frac{(-1)^{(m-2)}(m-2)!}{(-\mu)^{(m-1)}}E_m(\mu a), \end{aligned} \tag{5.11}$$

where $E_m(x)$ is the exponential integral function and defined as

$$E_m(x) = \int_1^\infty \frac{e^{-xt}}{t^m}dt. \tag{5.12}$$

Finally, using (5.11) in (5.8) after simplifying gives

$$\begin{aligned} I_{(m-1)} &= I_{(m-2)} + e^{\mu a}E_m(\mu a), \\ &= I_0 + e^{\mu a}\left(\sum_{j=2}^{m}E_j(\mu a)\right). \end{aligned} \tag{5.13}$$

The integral I_0 can be evaluated from (5.4) and using [17, Eq. 4.337.1]

$$\begin{aligned} I_0 &= \mu \int_0^\infty \ln(y+a) e^{-\mu y} dy, \\ &= \ln(a) - e^{\mu a} E_i(-\mu a), \\ &= \ln(a) + e^{\mu a} E_1(\mu a), \end{aligned} \tag{5.14}$$

where, $E_i(-x) = -E_1(x)$. Substituting the above equation in (5.13), we get the final expression as follows

$$I_{m-1} = \ln(a) + e^{\mu a} \left(\sum_{j=1}^{m} E_j(\mu a) \right). \tag{5.15}$$

5.1.2 Capacity after Averaging over PDF of Y

Substituting (5.2) in (5.1) and taking the expectation with respect to the PDF of Y in (4.13) whose parameters are given in Section 4.3, we have

$$\begin{aligned} \bar{\mathcal{C}} &= \log_2(e) E\Big[\ln\Big(1+\gamma\Big)\Big], \\ &= \log_2(e) \int_0^\infty \ln\Big(1+\gamma\Big) p_Y(y) dy, \\ &= \log_2\left(1 + \frac{\sigma_n^2}{g\sigma_s^2}\right) - \log_2(e) \prod_{n=1}^{R} \left(\frac{\lambda_1}{\lambda_n}\right)^\alpha \sum_{k=0}^{\infty} \zeta_k \left[\int_0^\infty \ln\left(y + \frac{\sigma_n^2}{g\sigma_s^2}\right) \frac{y^{R\alpha+k-1} e^{\frac{-y}{\lambda_1}}}{\lambda_1^{R\alpha+k}\Gamma(R\alpha+k)} dy \right]. \end{aligned} \tag{5.16}$$

The integral in the above equation is of the form

$$I_{(m-1)} = \int_0^\infty \ln\Big(y+a\Big) \frac{y^{m-1} e^{-\mu y}}{\mu^{-m}\Gamma(m)} dy = e^{\mu a} \int_a^\infty \ln\Big(y\Big) \frac{(y-a)^{m-1} e^{-\mu y}}{\mu^{-m}\Gamma(m)} dy. \tag{5.17}$$

Thus, the final expression for the capacity averaged over the PDF of Y, after using (5.15) in (5.16), is given by

$$\bar{\mathcal{C}} = \log_2\left(1 + \frac{\sigma_n^2}{g\sigma_s^2}\right) - \log_2(e) \prod_{n=1}^{R} \left(\frac{\lambda_1}{\lambda_n}\right)^\alpha \sum_{k=0}^{\infty} \zeta_k \left[\ln\left(\frac{\sigma_n^2}{g\sigma_s^2}\right) + e^{\frac{\sigma_n^2}{g\sigma_s^2\lambda_1}} \left(\sum_{j=1}^{R\alpha+k} E_j\left(\frac{\sigma_n^2}{g\sigma_s^2\lambda_1}\right) \right) \right]. \tag{5.18}$$

Jensen Approximation of (5.16)

The capacity derived in (5.18) is expressed in terms of exponential integral functions. There are, however, a couple of drawbacks associated with this expression. One is to do with the computational complexity because of the number and order of exponential integral functions

increases with the index k. The other is that, in order to determine the average capacity, we need to integrate (5.18) over the PDF of the random variable G which can be mathematically intractable. We, thus, resort to determine a simpler expression for (5.18).

Since we know that $0 \leq Y \leq 1$, we may expect that the PDF of Y to be narrow over this region which is quantified by its parameters $R\alpha + k$ and λ_1. As mentioned in Remark 4.3.1, $\lambda_1 \propto f_{3dB}/f_{sub}$ and, thus, for moderate levels of phase noise, the PDF will be narrow as seen in Fig. 4.1. The logarithm in the above integral, over this range of the PDF, will be a linear function and hence we could use the Jensen's inequality for the above integral which will be a good approximation, i.e.,

$$E\left[\ln(y+a)\right] \approx \ln\left(E\left[y\right]+a\right). \tag{5.19}$$

Applying the above Jensen approximation to (5.16), the integral can be approximated as

$$\begin{aligned}\int_0^\infty \ln\left(y+\frac{\sigma_n^2}{g\sigma_s^2}\right)\frac{y^{R\alpha+k-1}e^{\frac{-y}{\lambda_1}}}{\lambda_1^{R\alpha+k}\Gamma(R\alpha+k)}dy &\approx \ln\left(\frac{\sigma_n^2}{g\sigma_s^2}+\int_0^\infty \frac{y^{R\alpha+k}e^{\frac{-y}{\lambda_1}}}{\lambda_1^{R\alpha+k}\Gamma(R\alpha+k)}\right),\\ &= \ln\left(\frac{\sigma_n^2}{g\sigma_s^2}+\frac{\Gamma(R\alpha+k+1)\lambda_1}{\Gamma(R\alpha+k)}\right),\end{aligned} \tag{5.20}$$

where $\Gamma(\cdot)$ is the gamma function and $\int_0^\infty x^{v-1}e^{-\mu x}dx = \mu^{-v}\Gamma(v)$ [17, Eq. 3.381.4] was used in arriving at the above equation. Using (5.20) in (5.16), the capacity averaged over the PDF of Y becomes

$$\bar{\mathcal{C}} = \log_2\left(1+\frac{\sigma_n^2}{g\sigma_s^2}\right) - \prod_{n=1}^{R}\left(\frac{\lambda_1}{\lambda_n}\right)^\alpha \sum_{k=0}^{\infty}\zeta_k \log_2\left(\frac{\sigma_n^2}{g\sigma_s^2}+\frac{\Gamma(R\alpha+k+1)\lambda_1}{\Gamma(R\alpha+k)}\right). \tag{5.21}$$

Writing $K = \prod_{n=1}^{R}\left(\frac{\lambda_1}{\lambda_n}\right)^\alpha$, (5.21) can equivalently be written as

$$\begin{aligned}\bar{\mathcal{C}} &= \log_2\left(1+\frac{g\sigma_s^2}{\sigma_n^2}\right)+\log_2\left(\frac{\sigma_n^2}{g\sigma_s^2}\right)+\log_2\left[\prod_{k=0}^{\infty}\left(\frac{\sigma_n^2}{g\sigma_s^2}+\frac{\Gamma(R\alpha+k+1)\lambda_1}{\Gamma(R\alpha+k)}\right)^{-K\zeta_k}\right],\\ &= \log_2\left(1+\frac{g\sigma_s^2}{\sigma_n^2}\right)+\log_2\left[\prod_{k=0}^{\infty}\left(\frac{\sigma_n^2}{g\sigma_s^2}+\frac{\Gamma(R\alpha+k+1)\lambda_1}{\Gamma(R\alpha+k)}\right)^{-K\zeta_k}\left(\frac{\sigma_n^2}{g\sigma_s^2}\right)\right],\end{aligned} \tag{5.22}$$

from which we get the final expression as

$$\bar{\mathcal{C}} = \log_2\left(1+\frac{g\sigma_s^2}{\sigma_n^2}\right) - K\sum_{k=0}^{\infty}\zeta_k\left[\log_2\left(\left(\frac{\sigma_n^2}{g\sigma_s^2}\right)^{\frac{K\zeta_k-1}{K\zeta_k}}+\frac{\Gamma(R\alpha+k+1)\lambda_1}{\Gamma(R\alpha+k)}\left(\frac{g\sigma_s^2}{\sigma_n^2}\right)^{\frac{1}{K\zeta_k}}\right)\right], \tag{5.23}$$

where $K = \prod_{n=1}^{R}(\frac{\lambda_1}{\lambda_n})^\alpha$, $R = N_c - 1$, $\alpha = \frac{1}{2}$. As seen in (5.23), the capacity expression

consists of two terms: The first term is the capacity in an AWGN channel and the second term arises because of the phase noise. As expected, the net effect is a reduction from the AWGN capacity.

5.1.3 Average Capacity

We next average $\bar{\mathcal{C}}$ in (5.23) over the PDF of G to get the average capacity in block-fading channel. Assuming Rayleigh fading, G follows an exponential distribution with average value $\bar{g}$ and its PDF is given by

$$p_G(g) = \frac{1}{\bar{g}} e^{-\frac{g}{\bar{g}}}. \tag{5.24}$$

We start by averaging (5.21) over the PDF of G. Denoting $p = \frac{\sigma_n^2}{\sigma_s^2}$, $K = \prod_{n=1}^{R} (\frac{\lambda_1}{\lambda_n})^{\alpha}$ and $b_k = \frac{\Gamma(R\alpha+k+1)\lambda_1}{\Gamma(R\alpha+k)}$, (5.21) can be written as

$$\begin{aligned}
\bar{\mathcal{C}} &= \log_2(e) \left(\ln\left(1+\frac{p}{g}\right) - K \sum_{k=0}^{\infty} \zeta_k \ln\left(\frac{p}{g} + b_k\right)\right), \\
&= \log_2(e) \left(\ln(p+g) - \ln(g) - K \sum_{k=0}^{\infty} \zeta_k \left(\ln(p) + \ln\left(1+g\frac{b_k}{p}\right) - \ln(g)\right)\right), \\
&= \log_2(e) \left(\ln\left(1+\frac{g}{p}\right) + \ln(g)\left(K\sum_{k=0}^{\infty}\zeta_k - 1\right) - K\sum_{k=0}^{\infty}\zeta_k \left[\ln\left(1+g\frac{b_k}{p}\right)\right] \right. \\
&\qquad \left. + \ln(p)\left(1 - K\sum_{k=0}^{\infty}\zeta_k\right)\right).
\end{aligned} \tag{5.25}$$

Averaging the above equation over the PDF in (5.24), we get the expression for the average capacity as

$$\begin{aligned}
\bar{\bar{\mathcal{C}}} &= E\left[\bar{\mathcal{C}}\right], \\
&= \int_0^{\infty} \bar{\mathcal{C}} p_G(g) dg, \\
&= \log_2(e) \left[\left(1 - K\sum_{k=0}^{\infty}\zeta_k\right)\left(\ln\left(\frac{\sigma_n^2}{\bar{g}\sigma_s^2}\right) + \mathcal{E}\right) - e^{\frac{\sigma_n^2}{\bar{g}\sigma_s^2}} Ei\left(\frac{-\sigma_n^2}{\bar{g}\sigma_s^2}\right) + K\sum_{k=0}^{\infty}\zeta_k e^{\frac{\sigma_n^2}{\bar{g}b_k\sigma_s^2}} Ei\left(\frac{-\sigma_n^2}{\bar{g}b_k\sigma_s^2}\right)\right],
\end{aligned} \tag{5.26}$$

where $\mathcal{E} \approx 0.577215$ is the Euler's constant, $Ei(\cdot)$ is the exponential integral and $b_k = \frac{\Gamma(R\alpha+k+1)\lambda_1}{\Gamma(R\alpha+k)}$. In arriving at (5.26), we employed the following identities: $\int_0^{\infty} \log(x) e^{-\mu x} dx = -\frac{1}{\mu}(\mathcal{E} + \log(\mu))$ and $\int_0^{\infty} \log(1+\beta x) e^{-\mu x} dx = -\frac{1}{\mu} e^{\frac{\mu}{\beta}} Ei(\frac{-\mu}{\beta})$ [17, Eq. (4.331.1) and (4.337.2)].

5.2 SINR

The average SINR is obtained by first averaging γ given in (3.23) over the PDF of Y and then over the PDF of G. Taking the expectation of (3.23) with respect to the PDF of Y, we have

$$\begin{aligned}\bar{\gamma} &= E\left[\gamma\right], \\ &= \int_0^\infty \frac{1}{\frac{\sigma_n^2}{g\sigma_s^2}+y} p_Y(y)dy - \int_0^\infty \frac{y}{\frac{\sigma_n^2}{g\sigma_s^2}+y} p_Y(y)dy. \end{aligned} \tag{5.27}$$

Substituting the PDF of (4.13) in the above equation, and making use of $\int_0^\infty \frac{x^{v-1}e^{-\mu x}}{x+b}dx = b^{v-1}e^{b\mu}\Gamma(v)\Gamma(1-v,b\mu)$ [17, Eq. (3.383.10)], (5.27) can be simplified to

$$\begin{aligned}\bar{\gamma} = K\Big[\sum_{k=0}^{\infty} \zeta_k e^{(\frac{\sigma_n^2}{g\sigma_s^2\lambda_1})}(\frac{\sigma_n^2}{g\sigma_s^2\lambda_1})^{R\alpha+k-1}\frac{\Gamma_u\Big(1-(R\alpha+k),\frac{\sigma_n^2}{g\sigma_s^2\lambda_1}\Big)}{\lambda_1} - \\ \sum_{k=0}^{\infty} \zeta_k e^{(\frac{\sigma_n^2}{g\sigma_s^2\lambda_1})}(\frac{\sigma_n^2}{g\sigma_s^2\lambda_1})^{R\alpha+k}\Gamma_u\Big(-(R\alpha+k),\frac{\sigma_n^2}{g\sigma_s^2\lambda_1}\Big)(R\alpha+k)\Big],\end{aligned} \tag{5.28}$$

where $\Gamma_u(\cdot,\cdot)$ is the upper incomplete gamma function. The continued fraction representation of the incomplete gamma function is given as [1, Eq (6.5.31)]

$$\Gamma_{cf} = x^{-a}e^x\Gamma_u(a,x) = \left(\frac{1}{x+}\frac{1-a}{1+}\frac{1}{x+}\frac{2-a}{1+}\ldots\right). \tag{5.29}$$

Using (5.29) in (5.28), we can write the final expression for the SINR averaged over distribution of Y as

$$\bar{\gamma} = K\sum_{k=0}^{\infty}\zeta_k\left(\frac{\Gamma_{cf}\Big(1-(R\alpha+k),\frac{\sigma_n^2}{g\sigma_s^2\lambda_1}\Big)}{\lambda_1} - \Gamma_{cf}\Big(-(R\alpha+k),\frac{\sigma_n^2}{g\sigma_s^2\lambda_1}\Big)(R\alpha+k)\right), \tag{5.30}$$

where as before $K = \prod_{n=1}^{R}(\frac{\lambda_1}{\lambda_n})^\alpha$, $R = N_c - 1$ and $\alpha = \frac{1}{2}$. From (5.30), it is seen that $\bar{\gamma}$ depends on the phase noise process through λ_1 and on the ratio of the eigenvalues through ζ_k which are given in (4.17).

The average SINR is obtained by averaging $\bar{\gamma}$ in (5.30) over the PDF of G. A closed-form expression, however, is mathematically intractable. However, at high SNR, the average SINR can be derived because (3.23) can then be approximated closely as

$$\gamma_\infty \approx \frac{1-y}{y}. \tag{5.31}$$

This reflects the contribution of only the phase noise process to the SINR. Finally, averaging (5.31) over the PDF of Y in (4.13) and making use of $\int_0^\infty x^{v-1}e^{-\mu x}dx = \mu^{-v}\Gamma(v)$ [17, Eq

(3.381.4)], the expression for the average SINR at high SNR is obtained as

$$\bar{\gamma}_{\infty} = \bar{\bar{\gamma}}_{\infty} = \left[K \sum_{k=0}^{\infty} \zeta_k \left(\frac{\Gamma(R\alpha + k - 1)}{\Gamma(R\alpha + k)\lambda_1} \right) \right] - 1. \tag{5.32}$$

Most previous methods of evaluating the average SINR have been based on obtaining accurate second-order statistics of the CPE and ICI. From the system model given in (3.19) and repeated below

$$r_j = H_j \delta_0 s_j + H_j \sum_{k=0, k \neq j}^{N_c - 1} \delta_{k-j} s_k + n_j, \tag{5.33}$$

the average SINR is typically evaluated by taking the expectation of the magnitude square of the above equation and then taking the ratio of the desired signal power and the interfering noise power [40,41,49]. This measure of the SINR is accurate only if the desired signal and noise parts are independent of each other which is not the case when we have phase noise. Thus, evaluating the average SINR by this method, from (5.33), the average power of the j^{th} received subcarrier, while assuming the transmitted symbols $\{s_j\}_{j=0}^{N_c-1}$ are independent of each other, is given by

$$E\left[|r_j|^2\right] = E\left[|H_j|^2\right] E\left[|\delta_0|^2\right] \sigma_s^2 + E\left[|H_j|^2\right] \sum_{k=0, k \neq j}^{N_c - 1} E\left[|\delta_{k-j}|^2\right] \sigma_s^2 + \sigma_n^2, \tag{5.34}$$

where independence between the phase noise process, the channel is also assumed. Dropping the subscript j without loss of generality, the average SINR is obtained as

$$\begin{aligned} \bar{\gamma}_{est} &= \frac{E\left[|H|^2\right] E\left[|\delta_0|^2\right] \sigma_s^2}{E\left[|H|^2\right] E\left[\sum_{k=1}^{N_c-1} |\delta_k|^2\right] \sigma_s^2 + \sigma_n^2}, \\ &= \frac{1 - \bar{Y}}{\bar{Y} + \frac{\sigma_n^2}{\bar{g}\sigma_s^2}}, \end{aligned} \tag{5.35}$$

where $\bar{g} = E\left[|H|^2\right]$, $|\delta_0|^2 = 1 - Y$, $Y = \sum_{k=1}^{N_c-1} |\delta_k|^2$ and $\bar{Y}$ denotes the mean of Y and is given by (4.29). In Chapter 6, we compare the average SINR estimates of (5.35) and (5.30). Since (5.30) was derived under the assumption of a fixed channel, the $\bar{g}$ in the denominator of (5.35) would now be a fixed realization when we do the comparison. We show that (5.35) is a poor estimate of the average SINR.

5.3 Outage Capacity with Fixed G

The outage capacity is typically defined as the maximum bit rate $\mathcal{C}_{out}$ with probability of outage equal to q, i.e., $P_{\mathcal{C}}(\mathcal{C} < \mathcal{C}_{out}) = q$ from which the outage capacity is obtained as

$$\mathcal{C}_{out} = P_{\mathcal{C}}^{-1}(q), \tag{5.36}$$

where $P_{\mathcal{C}}(\cdot)$ is the cumulative distribution function (CDF) of $\mathcal{C}$. From the definition of the capacity in (5.1), to which it is related to Y through (3.23), we can equivalently expresses the probability of outage of $\mathcal{C}$ in terms of Y as follows

$$\begin{aligned} P_{\mathcal{C}}(\mathcal{C} < \mathcal{C}_{out}) &= q \implies P_Y\left(\frac{1-y}{y+\frac{\sigma_n^2}{g\sigma_s^2}} < \frac{1-y_{out}}{y_{out}+\frac{\sigma_n^2}{g\sigma_s^2}}\right) = q, \\ &= 1 - P_Y(Y < y_{out}) = q. \end{aligned} \tag{5.37}$$

Thus, y_{out} is given as

$$y_{out} = P_Y^{-1}(1-q), \tag{5.38}$$

where $P_Y(\cdot)$ is the CDF of Y and is obtained by integrating over its PDF in (4.13) as

$$\begin{aligned} P_Y(Y < y) &= \int_0^y p_Y(t)dt, \\ &= K\int_0^y \sum_{k=0}^{\infty} \frac{\zeta_k t^{R\alpha+k-1} e^{\frac{-t}{\lambda_1}}}{\lambda_1^{R\alpha+k}\Gamma(R\alpha+k)} dt, \\ &= K\sum_{k=0}^{\infty} \zeta_k \frac{\Gamma_l(R\alpha+k, \frac{y}{\lambda_1})}{\Gamma(R\alpha+k)}, \end{aligned} \tag{5.39}$$

where $\Gamma_l(\cdot,\cdot)$ is the lower incomplete gamma function. Using (3.23), (5.1), and (5.38), the expression for the outage capacity in a fixed channel is given as

$$\mathcal{C}_{out} = \log_2\left(1 + \frac{1-y_{out}}{y_{out} + \sigma_n^2/(g\sigma_s^2)}\right). \tag{5.40}$$

An explicit expression for y_{out} is difficult to derive as the inverse function P_Y^{-1} does not exist in the general case and, hence, we evaluate it numerically. In following chapter, we compare the analytical expressions derived in this chapter with the simulations alongside discussions on the inferences of the results.

Chapter 6

Numerical Results

In this chapter, we present the Monte Carlo simulations of the SINR and capacity. We present two cases. In the first, the analytical performance measures derived in Chapter 5 are compared with the simulations in Section 6.2. The analytical performance measures of SINR and capacity were derived on a per-subcarrier basis and, hence, it does not reflect the net throughput of the system. Thus, in Section 6.3, we present the simulations of the net throughput and analyze its behavior in the context of phase noise. In Section 6.1, we explain the system setups used in the simulations of Sections 6.2 and 6.3.

6.1 System Setup

For the Monte Carlo simulations in Section 6.2, we consider an OFDM system with bandwidth 20MHz and $N_c = 1024$ subcarriers given the subcarrier spacing $f_{sub} = 19.5$kHz. For obtaining the analytical performance measures, we need the eigenvalues which are obtained from the square-root of the normalized covariance matrix $\mathbf{M_z}$ of the gamma variables in (4.1). The number of gamma RVs is $N = \frac{N_c(N_c-1)}{2}$ and, hence, the number of elements in $\mathbf{M_z}$, with $N_c = 1024$, is in the order of 10^{10}. Obtaining the eigenvalues for such a large matrix is practically infeasible mainly due to memory storage issues. However, as long as f_{3dB} is small compared to f_{sub}, there is negligible ICI between subcarriers that are very far apart. Thus, without causing any significant change to the ICI term, we can reduce N_c while keeping f_{sub} fixed, thereby reducing the bandwidth. Hence, without loss of accuracy, we may evaluate the analytical performance measures with $N_c = 32$, $f_{sub} = 19.5$kHz and bandwidth of 625kHz.

For evaluating the net throughput in Section 6.3, the bandwidth of the OFDM system is 20MHz. We might be inclined to believe that the net throughput, in the absences of phase noise, would increase as the number of subcarriers increases as more data is transmitted

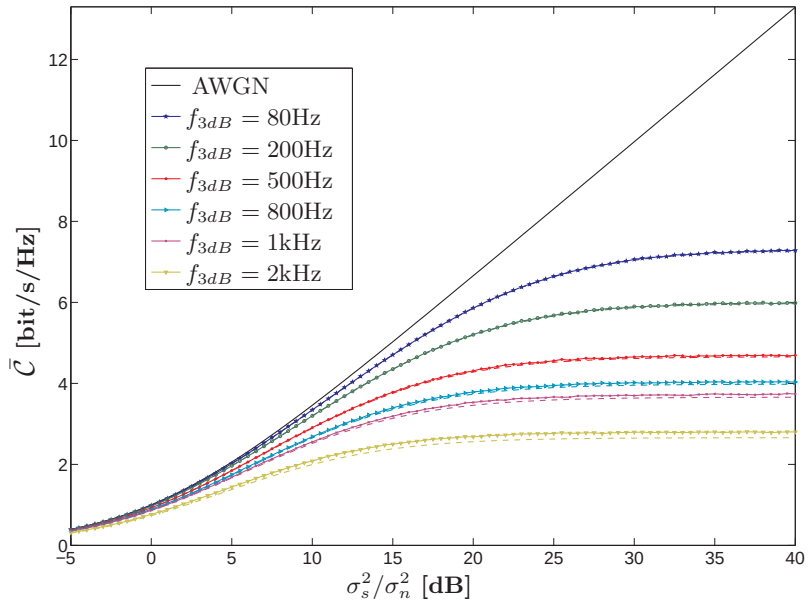

Figure 6.1: Comparison between simulated and analytical capacity $\bar{\mathcal{C}}$ plots with fixed g=1. The dashed lines represent the analytical results and the solid marker lines represent the simulations.

in parallel. It is, thus, interesting to see the effect of the number of subcarriers on the net throughput. Hence, for the simulations of the net throughput, we vary the number of subcarriers from as low as two subcarriers to a maximum of two thousand forty eight subcarriers. Again, as mentioned in the earlier paragraph, presenting the analytical net throughput for subcarriers even larger than thirty two can be quite demanding in terms of memory. Hence, we omit the presentation of the analytical throughput.

6.2 Capacity and SINR per Subcarrier

Figures 6.1 and 6.2 show the plots for $\bar{\mathcal{C}}$ (capacity averaged over PDF of Y) and $\bar{\bar{\mathcal{C}}}$ (capacity averaged over PDFs of both Y and G), respectively. The capacity with phase noise in both figures is compared with the AWGN capacity. The impact of phase noise is clearly visible on the capacity and the analytical capacities derived in (5.23) and (5.26) predict well the simulation results. We see that, for any given f_{sub} and σ_s^2/σ_n^2, increasing f_{3dB} decreases the capacity. This is also evident from (5.23) and (5.26). As seen in (5.23), $\bar{\mathcal{C}}$ indirectly depends on N_c, f_{sub} and the f_{3dB} through λ_1, K and ζ_k. As earlier mentioned, $\{\lambda_n\}_{n=1}^{R}$ are proportional to σ^2 of (3.26). The ratio λ_1/λ_n is independent of σ^2 and N_c, hence, K and ζ_k too. Thus, $\bar{\mathcal{C}}$ in (5.23) depends only on λ_1 and as f_{3dB}/f_{sub} increases, λ_1 increases and $\bar{\mathcal{C}}$, thus, decreases. Similarly, $\bar{\bar{\mathcal{C}}}$, in (5.26), depends on λ_1 which is an argument of the

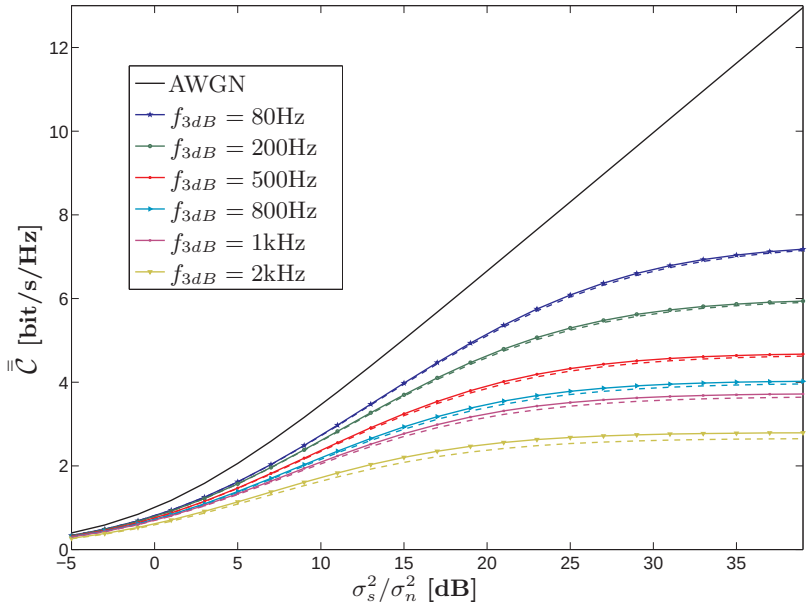

Figure 6.2: Comparison between simulated and analytical $\bar{\bar{\mathcal{C}}}$ plots. The channel is Rayleigh fading with $\bar{g} = 1$. The dashed lines represent the analytical results and the solid marker lines represent the simulations.

exponential and the exponential integral function. As λ_1 increases, the exponential and the exponential integral functions decrease, thereby, decreasing the capacity.

From Fig. 6.2, we see that capacity is decreased once fading is taken into account. However, this effect is more pronounced in the low to midrange SNRs. At very high SNRs, there is practically no difference between the curves of Fig. 6.1 and Fig. 6.2 which can be proved as follows. At high SNRs, from (5.31), we see that there is no effect of the channel on the capacity which now depends only on phase noise process. We can use (5.20), again assuming that f_{3dB}/f_{sub} is small, to derive the capacity at high SNR as

$$\bar{\mathcal{C}}_\infty = \bar{\bar{\mathcal{C}}}_\infty = K \sum_{k=0}^{\infty} \zeta_k \left[\log_2 \left(\frac{\Gamma(R\alpha + k)}{\Gamma(R\alpha + k + 1)\lambda_1} \right) \right]. \tag{6.1}$$

From Figs. 6.1 and 6.2, we see that, for $f_{3dB} = 2$kHz, there is a minor difference between the analytical and simulated capacities. This is attributed to the fact that the Taylor series approximation starts breaking down. As mentioned in Section 4.1, σ^2_{max} given by (4.9) characterizes the accuracy of the approximation. It is, thus, imperative to see its effect on the prediction of the capacity by the analysis done so far. Figure 6.3 shows the plots of $\bar{\mathcal{C}}$ in terms of σ^2_{max} for four different SNR values. The plot for $\sigma_s^2/\sigma_n^2 = \infty$ corresponds to $\bar{\mathcal{C}}_\infty = \bar{\bar{\mathcal{C}}}_\infty$ of (6.1). We can conclude that the achievable capacity for a given SNR

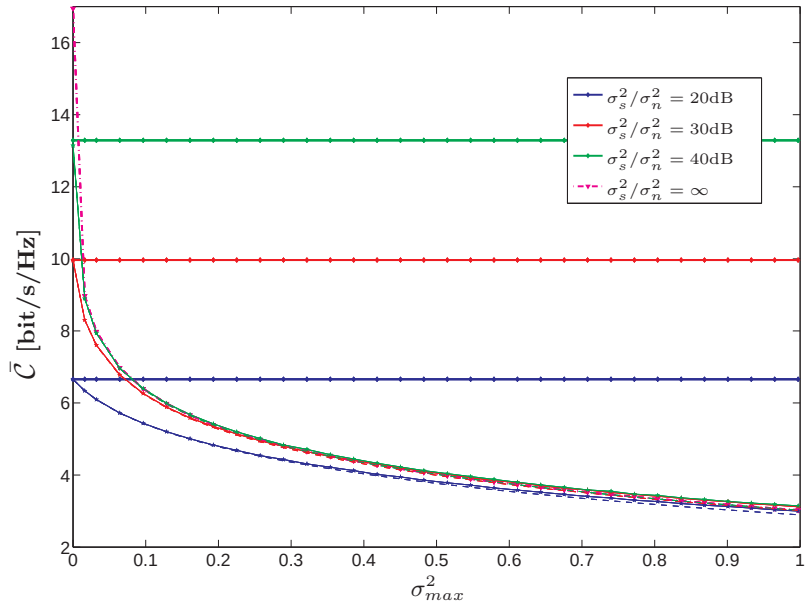

Figure 6.3: Comparison between simulated and analytical $\bar{\mathcal{C}}$ plots with fixed g=1. The respective dashed, solid star and solid diamond lines represent the analytical results, simulation results and the AWGN channel capacity.

clearly depends mainly on the ratio of f_{3dB} and f_{sub} which agrees with intuition. Also, the analytical capacities predict the simulations well even for σ^2_{max} as large as one, which corresponds to $f_{sub} = 4\pi f_{3db}$ by (4.9). Thus, if $f_{sub} \geq 4\pi f_{3dB} \approx 10 f_{3dB}$ then we are well within the limits for which the Taylor series approximation holds.

Figure 6.4 shows the average SINR plots for $\bar{\gamma}$ of (5.30) and $\bar{\gamma}_{est}$ of (5.35) and compares them with Monte Carlo simulations. Clearly, we see that $\bar{\gamma}_{est}$ is poor estimate of the average SINR and does not match with Monte Carlo simulations. Thus, this reaffirms the fact that complete knowledge of the distribution of ICI power in (3.23) is necessary to get accurate estimate of the statistics of the SINR and functions derived from it. The closeness between the simulation and analytical plots of $\bar{\gamma}$ here is better than in the capacity plots of Figs. 6.1 and 6.2. This is because no kind of approximation was used in arriving at $\bar{\gamma}$ in (5.30) but the Jensen approximation was used in order to arrive at the analytical capacity in (5.23). Also, as with the capacity, we see saturation of $\bar{\gamma}$ at high SNRs. For such high SNRs, $\bar{\gamma}$ converges to $\bar{\gamma}_\infty = \bar{\bar{\gamma}}_\infty$ given in (5.32).

Figure 6.5 shows the outage capacity plots for $\mathcal{C}_{out}$ of (5.40). We see that there is larger deviation between the analytical and the simulation results for the same f_{3dB} used in the capacity and SINR plots. This is expected because the CDF of Y is more in error when compared to the PDF, which was derived using the Taylor series approximation, since any error in the PDF accumulates into the CDF because of the integration operation. Any

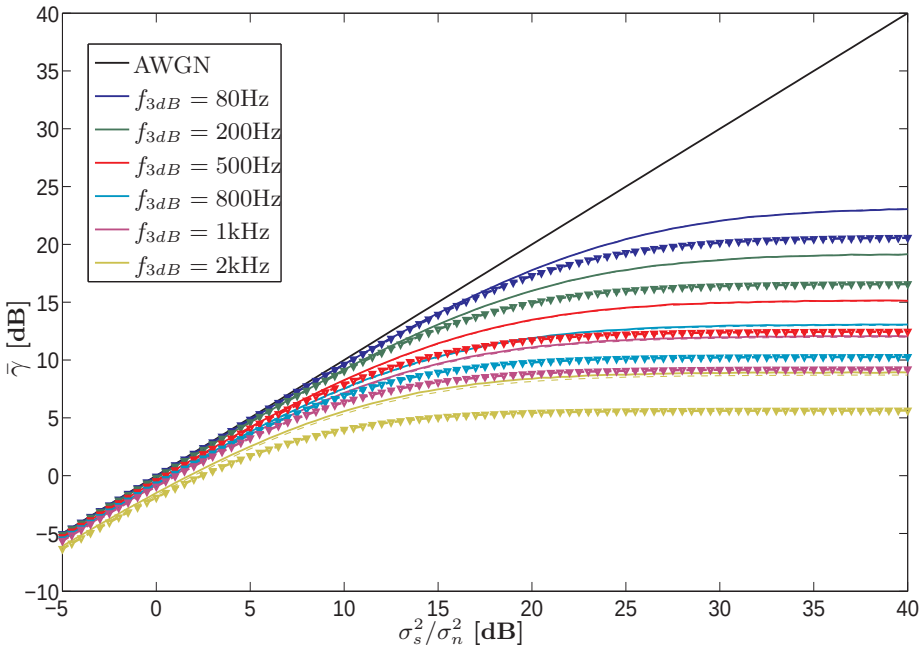

Figure 6.4: Comparison between simulated and analytical average SINR plots with fixed g=1. The dashed lines represent the analytical $\bar{\gamma}$ of (5.30) and the solid lines represent its corresponding Monte Carlo simulations. The marker lines denote $\bar{\gamma}_{est}$ of (5.35).

performance measure based on the CDF will, thus, be higher in error when compared to performance measures based on the PDF.

6.3 Net Throughput

In the previous section, we compared the analytical results of the average capacity and SINR with the simulations. However, the capacity derived was illustrated on a per-subcarrier basis which does not reflect the net throughput of the OFDM system impaired phase noise. To obtain the net throughput, we need to multiply $\bar{\mathcal{C}}$ (or $\bar{\bar{\mathcal{C}}}$ if we consider the channel) by the number of subcarriers and divide it by the time duration of the OFDM symbol which is $T = (N_c + N_{cp})T_s$. Here N_{cp} and T_s denote the respective cyclic prefix length and the sampling period. As mentioned in Chapter 2, cyclic prefix is added to combat the effect of ISI introduced by the multi-path channel. It introduces overhead into the system and results in a reduction of the net throughput of an AWGN channel as shown in Fig. 6.6.

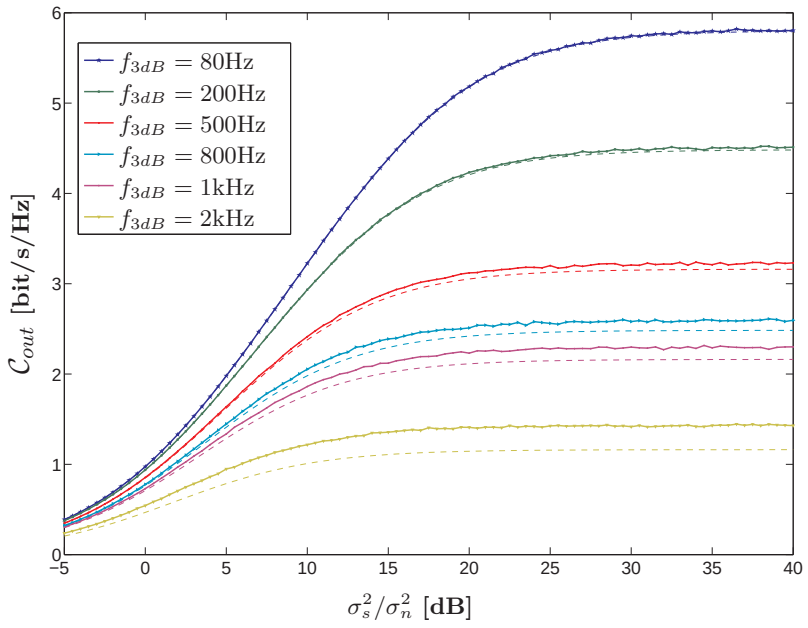

Figure 6.5: Comparison between simulated and analytical $\mathcal{C}_{out}$ plots with 10 percent outage probability and g=1. The dashed lines represent the analytical results and the solid marker lines represent the simulations.

The net throughput is, thus, given by

$$\begin{aligned} \bar{\mathcal{C}}_T &= \frac{\bar{\mathcal{C}}_{N_c}}{T}, \\ &= \frac{N_c \bar{\mathcal{C}} F_s}{N_c + N_{cp}}, \end{aligned} \tag{6.2}$$

where $F_s = 1/T_s$ is the sampling frequency. Using (5.23) in (6.2), we have the net throughput in terms of

$$\begin{aligned} \bar{\mathcal{C}}_T = &\left(\frac{N_c F_s}{N_c + N_{cp}}\right) \log_2\left(1 + \frac{g\sigma_s^2}{\sigma_n^2}\right) \\ &- K\left(\frac{N_c F_s}{N_c + N_{cp}}\right) \sum_{k=0}^{\infty} \zeta_k \left[\log_2\left(\left(\frac{\sigma_n^2}{g\sigma_s^2}\right)^{\frac{K\zeta_k - 1}{K\zeta_k}} + \frac{\Gamma(R\alpha + k + 1)\lambda_1}{\Gamma(R\alpha + k)}\left(\frac{g\sigma_s^2}{\sigma_n^2}\right)^{\frac{1}{K\zeta_k}}\right)\right]. \end{aligned} \tag{6.3}$$

Figure 6.6 shows the Monte Carlo simulations of $\bar{\mathcal{C}}_T$ vs. the number of subcarriers for different 3dB bandwidths of the phase noise process and different cyclic prefix lengths. We have not plotted the analytical $\bar{\mathcal{C}}_T$, again due to memory storage issues in computing the $\mathbf{M_x}$ matrix. From Fig. 6.6, the maximum throughput is achieved for the AWGN case and in the absence of phase noise. This is achieved for $N_{cp} = 0$ or, for a given N_{cp}, choosing $N_c \gg N_{cp}$ as seen in Fig. 6.6. This behavior is easily evident from (6.3) for the AWGN

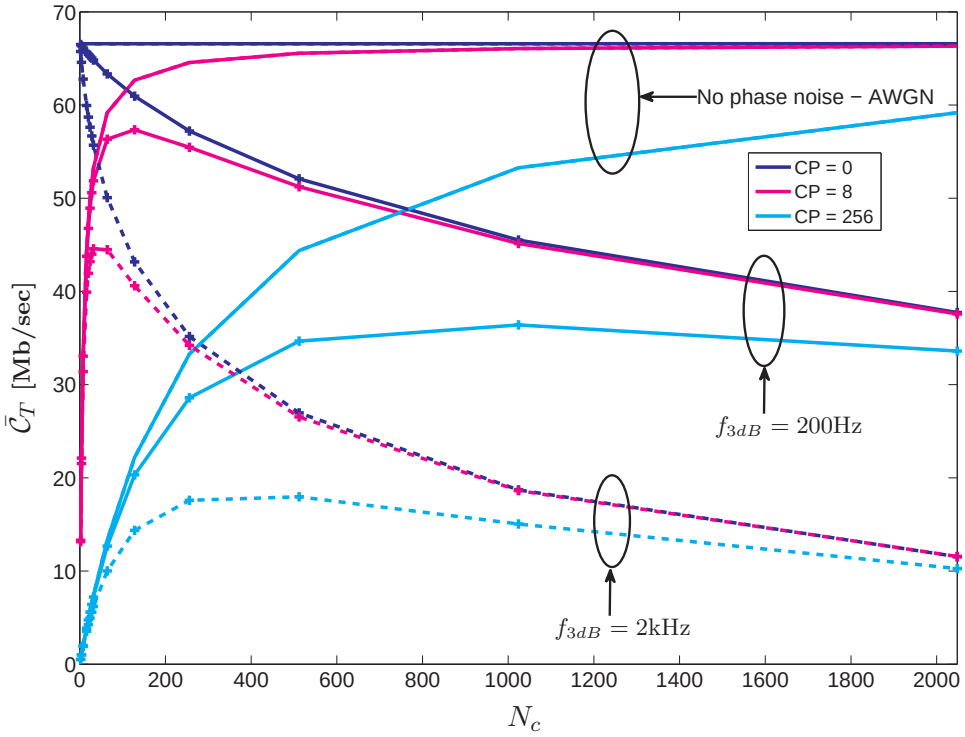

Figure 6.6: $\bar{C}_T$ vs. N_c. Bandwidth of the OFDM system is 10MHz with SNR of 20dB.

case (the summation term is zero). The addition of cyclic prefix to combat the multipath nature of the channel and its effect of ISI results in a reduction of the net throughput in an AWGN channel with $N_{cp} = 0$. We can minimize this loss by increasing the number of subcarriers. However, the scenario worsens when we have phase noise, because we know that, for a fixed bandwidth, increasing N_c (and hence reducing f_{sub}) reduces the capacity as evidenced in Fig. 6.3. Thus, we have two conflicting scenarios, where for a given N_{cp}, increasing N_c decreases the relative overhead due to cyclic prefix, while at the same time, the phase noise decreases the SINR and hence the throughput.

From (6.3), for a given SNR and N_{cp}, both the first and second terms increase with N_c with the rate of increase being slower for the second term. However, the first term in (6.3) represents the throughput in an AWGN channel which saturates after a certain N_c (see Fig. 6.6 for the AWGN case). This saturation does not take place for the second term as summation term increases with increasing N_c. We would then expect the net throughput to reach a maximum and then start decreasing after a certain value of N_c as evidenced in the figure. We, henceforth, call this maximal point as the optimal throughput $\bar{C}_{opt}$ and the subcarrier corresponding to it as the optimal number of subcarriers N_{copt}.

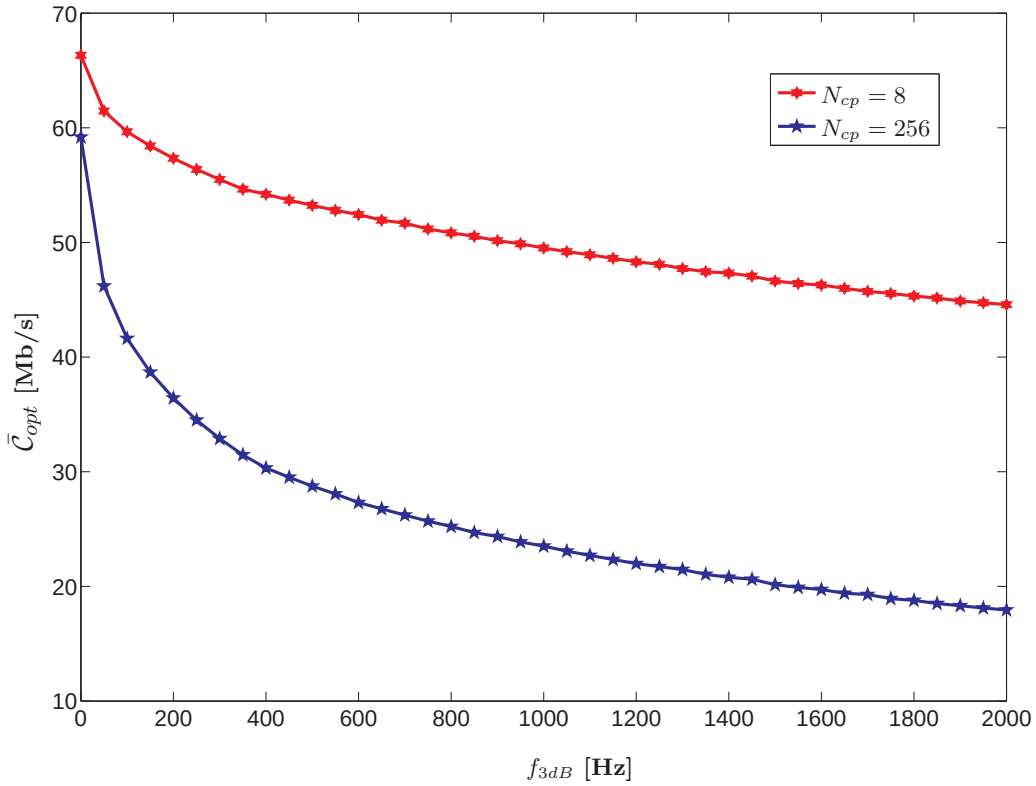

Figure 6.7: $\bar{\mathcal{C}}_{opt}$ vs. f_{3dB}. Bandwidth of the OFDM system is 10MHz with SNR of 20dB.

This is appropriate because it clearly tells for a given phase noise level, SNR and cyclic prefix length, the optimal number of subcarriers we should use to achieve the maximum throughput.

In Fig. 6.6, for a given cyclic prefix length, we see that the maximal point, i.e., $\bar{\mathcal{C}}_{opt}$ reduces when the f_{3dB} bandwidth increases. Intuition dictates that the optimal throughput decreases with increase in f_{3dB} which can also be seen from (6.3). Figure 6.7 exemplifies this behavior for different 3dB bandwidths of phase noise process.

Figure 6.8 shows the optimal number of subcarriers required to achieve the maximum throughput as a function of the 3dB bandwidth of the phase noise process. The figure clearly illustrates, for a given cyclic prefix length and SNR, how we should optimally choose the number of subcarriers, knowing the 3dB bandwidth of the phase noise process, so that the net throughput is maximized.

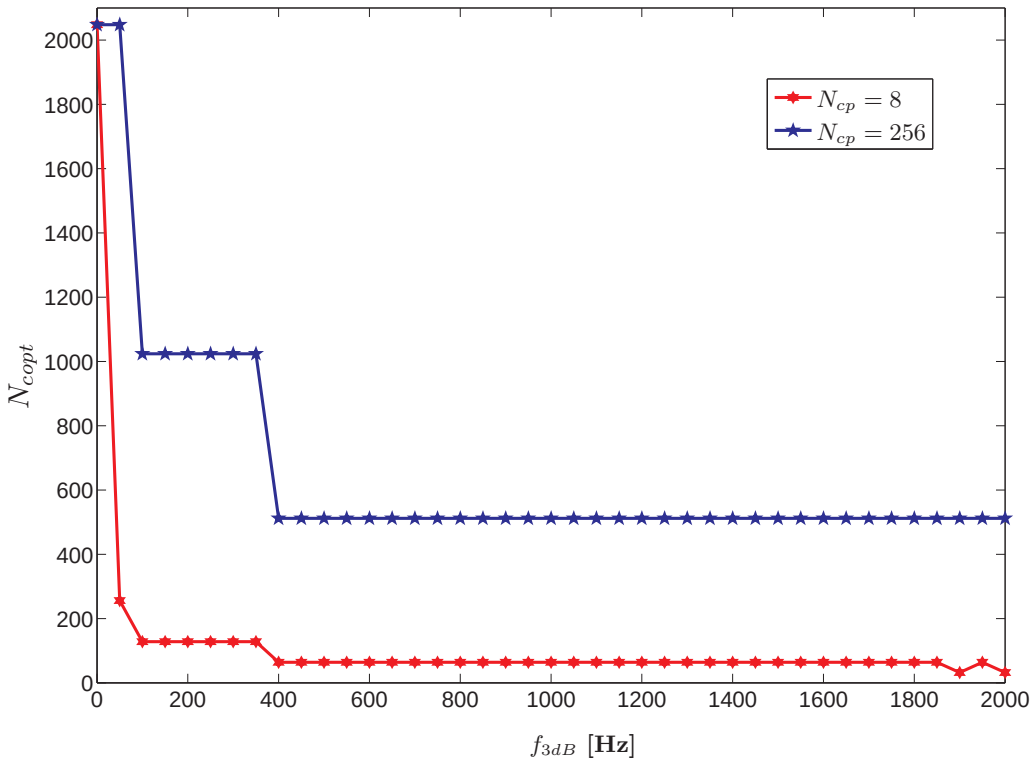

Figure 6.8: N_{copt} vs. f_{3dB}. Bandwidth of the OFDM system is 10MHz with SNR of 20dB.

Chapter 7

Conclusions

This thesis considers the effect of Wiener phase noise on the performance of OFDM systems. Analytical statistical expressions of capacity and SINR are derived and verified by the simulations. It is shown that the aforementioned performance metrics depend on the ratio of the subcarrier spacing and the 3dB bandwidth of the oscillator power spectral density. The performance degrades as this ratio becomes small. Thus, to achieve a given performance level, a trade off between the number of subcarriers and the type of oscillator need to be considered. In comparison to previous works on performance analysis of phase noise effects on OFDM, a probability density function based approach is employed. From the system model of OFDM in the presence of phase noise, it is seen that the SINR and capacity depend on two independent random variables, one characterizing the phase noise and the other the channel. The random variable characterizing the Wiener phase noise is shown to be a sum of correlated gamma variables (with rank-deficient square-root normalized covariance matrix) using a Taylor series approximation. The validity of the approximation depends on the ratio of the subcarrier spacing and the 3dB bandwidth of the oscillator power spectral density and holds well when this ratio is at least one order of magnitude, which for most standards and commercially available oscillators is the case. In earlier literature, the probability density function of a sum of correlated gamma variables with full-rank square-root normalized covariance matrix is derived. In this thesis, the generalization to the rank-deficient case is presented and applied to the random variable describing the Wiener phase noise process in the instantaneous SINR and capacity expressions.

7.1 Future Work

The analysis of this thesis is limited to Wiener phase noise process. Typically Wiener phase noise processes occur in free-running or autonomous oscillators which are basically

open loop voltage controlled oscillators. Most commercial oscillators typically are of the phase locked loop type. These involve feedback where the phase of a reference oscillator is compared with the phase of the voltage controlled oscillator and the phase difference drives the voltage controlled oscillator; in the ideal case of zero phase difference, no phase noise is present. In the more practical case, the resulting phase noise process is no longer of the Wiener type. Applying the analysis done in this work for this general class of oscillators would be area of research to pursue.

Bibliography

[1] M. Abramowitz and I. Stegun, *Handbook of Mathematical Functions with Formulas,Graphs and Mathematical Tables*. Dover Publications, 1972.

[2] M.-S. Alouini, A. Abdi, and M. Kaveh, "Sum of gamma variates and performance of wireless communication systems over Nakagami-fading channels," *IEEE Trans. Veh. Technol.*, vol. 50, no. 6, pp. 1471–1480, Nov. 2001.

[3] J. Barnes, "Models for the interpretation of frequency stability measurements," *Final Report National Bureau of Standards, Boulder, CO. Time and Frequency Div.*, Aug. 1976.

[4] S. Bittner, M. Krondorf, and G. Fettweis, "Numerical performance evaluation of OFDM systems affected by transmitter nonlinearities, phase noise and channel estimation errors," in *Proc. IEEE Global Telecommunications Conference (GLOBECOM'2008)*, Nov./Dec. 2008.

[5] A. Brajal and A. Chouly, "Compensation of nonlinear distortions for orthogonal multicarrier schemes using predistortion," in *IEEE Global Telecommunications Conference, 1994*, vol. 3, Nov. 1994, pp. 1909–1914.

[6] R. Casas, S. Biracree, and A. Youtz, "Time domain phase noise correction for OFDM signals," *IEEE Trans. Broadcast.*, vol. 48, no. 3, pp. 230–236, Sep. 2002.

[7] E. Costa, M. Midrio, and S. Pupolin, "Impact of amplifier nonlinearities on OFDM transmission system performance," *IEEE Commun. Lett.*, vol. 3, no. 2, pp. 37–39, Feb. 1999.

[8] E. Costa and S. Pupolin, "M-QAM-OFDM system performance in the presence of a nonlinear amplifier and phase noise," *IEEE Trans. Commun.*, vol. 50, no. 3, pp. 462–472, Mar. 2002.

[9] D. Dardari, V. Tralli, and A. Vaccari, "A theoretical characterization of nonlinear distortion effects in OFDM systems," *IEEE Trans. Commun.*, vol. 48, no. 10, pp. 1755–1764, Oct. 2000.

[10] A. Demir, "Phase noise and timing jitter in oscillators with colored-noise sources," *IEEE˙J˙CASI˙RP*, vol. 49, no. 12, pp. 1782–1791, Dec. 2002.

[11] A. Demir, A. Mehrotra, and J. Roychowdhury, "Phase noise in oscillators: A unifying theory and numerical methods for characterization," *IEEE Trans. Circuits Syst. I*, vol. 47, no. 5, pp. 655–674, May 2000.

[12] M. El-Tanany, Y. Wu, and L. Hazy, "Analytical modeling and simulation of phase noise interference in OFDM-based digital television terrestrial broadcasting systems," *IEEE Trans. Broadcast.*, vol. 47, no. 1, pp. 20–31, Mar. 2001.

[13] G. Fettweis, M. Lohning, D. Petrovic, M. Windisch, P. Zillmann, and W. Rave, "Dirty RF: A new paradigm," in *Proc. IEEE 16th International Symposium on Personal, Indoor and Mobile Radio Communications (PIMRC'2005)*, vol. 4, Sep. 2005, pp. 2347–2355.

[14] M. Frazier, *An Introduction to Wavelets Through Linear Algebra*. Springer, 1999.

[15] A. Garcia Armada, "Understanding the effects of phase noise in orthogonal frequency division multiplexing OFDM," *IEEE Trans. Broadcast.*, vol. 47, no. 2, pp. 153–159, Jun. 2001.

[16] C. Gardiner, *Handbook of stochastic methods for physics, chemistry, and the natural sciences, vol. 13 of Springer series in synergetics*. Springer-Verlag, second ed, 1983.

[17] I. Gradshteyn and I. Ryzhik, *Table of Integrals, Series, and Products*. Academic Press, 2007.

[18] S. Haykin, *Communication Systems*. New York Wiley, 2000.

[19] M. Jalloh, M. Al-Gharabally, and P. Das, "Performance of OFDM systems in Rayleigh fading channels with phase noise and channel estimation errors," in *Proc. IEEE Military Communications Conference (MILCOM'2006)*, Oct. 2006.

[20] M. Jalloh and P. Das, "Performance analysis of STBC-OFDM transmit diversity with phase noise and imperfect channel estimation," in *Proc. IEEE Military Communications Conference (MILCOM'2008)*, Nov. 2008.

[21] N. Johnson and S. Kotz, *Continous Multivariate Distributions*. New York Wiley, 1972.

[22] S. M. Kay, *Fundamentals of statistical signal processing: Volume 1, Estimation theory.* Prentice Hall, 1993.

[23] S. Kotz and J. Adams, "Distribution of sum of identically distributed exponentially correlated gamma-variables," *Ann. Inst. Statist. Math*, vol. 35, no. 1, pp. 277–283, Mar. 1964.

[24] C.-H. Liu, "Performance analysis of two-sided IQ imbalance effects in OFDM systems," in *IEEE 20th International Symposium on Personal, Indoor and Mobile Radio Communications, 2009*, Sep. 2009, pp. 938–942.

[25] P. Lombardo, G. Fedele, and M. Rao, "MRC performance for binary signals in Nakagami fading with general branch correlation," *IEEE Trans. Commun.*, vol. 47, no. 1, pp. 44–52, Jan. 1999.

[26] D. Luca Carni and D. Grimaldi, "Amplitude and phase noise measurement in single carrier digital modulations," in *Proceedings of the IEEE Instrumentation and Measurement Technology Conference, 2005. IMTC 2005.*, vol. 3, May 2005, pp. 1917–1922.

[27] S. Mallick and S. Majumder, "Performance analysis of an OFDM system in the presence of carrier frequency offset, phase noise and timing jitter over Rayleigh fading channels," in *Proc. IEEE International Conference on Electrical and Computer Engineering (ICECE'2008)*, Dec. 2008, pp. 205–210.

[28] P. Mathecken, T. Riihonen, S. Werner, and R. Wichman, "Performance analysis of OFDM with Wiener phase noise and frequency selective fading channel," *IEEE Trans. Commun.*, To appear 2011.

[29] A. Mehrotra, "Noise analysis of phase-locked loops," *IEEE Trans. Circuits Syst. I*, vol. 49, no. 9, pp. 1309–1316, Sep. 2002.

[30] K. S. Miller, *Multidimensional Gaussian Distributions.* John Wiley and Sons, 1964.

[31] J. Montojo and L. Milstein, "Effects of imperfections on the performance of OFDM systems," *IEEE Trans. Commun.*, vol. 57, no. 7, pp. 2060–2070, 2009.

[32] M. Morelli, A. D'Andrea, and U. Mengali, "Feedback frequency synchronization for OFDM applications," *IEEE Commun. Lett.*, vol. 5, no. 1, pp. 28–30, Jan. 2001.

[33] M. Morelli and U. Mengali, "An improved frequency offset estimator for OFDM applications," *IEEE Commun. Lett.*, vol. 3, no. 3, pp. 75–77, Mar. 1999.

[34] P. Moschopoulos, "The distribution of the sum of independent gamma random variables," *Ann. Inst. Statist. Math*, vol. 37, no. 1, pp. 541–544, Dec. 1985.

[35] C. Muschallik, "Influence of RF oscillators on an OFDM signal," in *Proc. IEEE International Conference on Consumer Electronics*, vol. 41, no. 3, Aug. 1995, pp. 592–603.

[36] K. Nikitopoulos and A. Polydoros, "Phase-impairment effects and compensation algorithms for OFDM systems," *IEEE Trans. Commun.*, vol. 53, no. 4, pp. 698–707, Apr. 2005.

[37] D. Petrovic, W. Rave, and G. Fettweis, "Intercarrier interference due to phase noise in OFDM — Estimation and suppression," in *Proc. IEEE 60th Vehicular Technology Conference (VTC'2004)*, vol. 3, Sep. 2004, pp. 2191–2195.

[38] ——, "Properties of the intercarrier interference due to phase noise in OFDM," in *2005 IEEE International Conference on Communications, ICC 2005.*, vol. 4, May 2005, pp. 2605–2610.

[39] ——, "Effects of phase noise on OFDM systems with and without PLL: Characterization and compensation," *IEEE Trans. Commun.*, vol. 55, no. 8, pp. 1607–1616, Aug. 2007.

[40] L. Piazzo and P. Mandarini, "Analysis of phase noise effects in OFDM modems," *IEEE Trans. Commun.*, vol. 50, no. 10, pp. 1696–1705, Oct. 2002.

[41] T. Pollet, M. Van Bladel, and M. Moeneclaey, "BER sensitivity of OFDM systems to carrier frequency offset and Wiener phase noise," *IEEE Trans. Commun.*, vol. 43, no. 234, pp. 191–193, Feb./Apr. 1995.

[42] J. Proakis, *Digital Communications*. Mc Graw Hill, 2000.

[43] B. Putra and G. Fettweis, "Clock jitter estimation and suppression in OFDM systems employing bandpass Sigma-Delta ADC," in *IEEE 10th Workshop on Signal Processing Advances in Wireless Communications, 2009. SPAWC '09.*, Jun. 2009, pp. 623–627.

[44] M. Rahman, D. Hossain, and S. Ali, "Performance analysis of OFDM systems with phase noise," in *Proc. IEEE 6th International Conference on Computer and Information Science (ICIS'2007)*, 2007, pp. 358–362.

[45] B. Razavi, "Design considerations for direct-conversion receivers," *IEEE Trans. Circuits Syst. II*, vol. 44, no. 6, pp. 428–435, Jun. 1997.

[46] J. Rinne and M. Renfors, "An equalization method for orthogonal frequency division multiplexing systems in channels with multipath propagation, frequency offset and phase noise," in *Global Telecommunications Conference, 1996. GLOBECOM '96.*, vol. 2, Nov. 1996, pp. 1442–1446.

[47] E. Rubiola, *Phase noise and frequency stability in oscillators.* Cambridge University Press, 2009.

[48] J. Rutman, "Characterization of phase and frequency instabilities in precision frequency sources: Fifteen years of progress," *Proceedings of the IEEE*, vol. 66, no. 9, pp. 1048–1075, 1978.

[49] H.-G. Ryu, Y. S. Li, and J.-S. Park, "Nonlinear analysis of the phase noise in the OFDM communication system," *IEEE Trans. Consum. Electron.*, vol. 50, no. 1, pp. 54–63, Feb. 2004.

[50] K. Sathananthan and C. Tellambura, "Performance analysis of an OFDM system with carrier frequency offset and phase noise," in *Proc. IEEE 54th Vehicular Technology Conference (VTC'2001)*, vol. 4, 2001, pp. 2329–2332.

[51] T. Schenk, R. van der Hofstad, E. Fledderus, and P. Smulders, "Distribution of the ICI term in phase noise impaired OFDM systems," *IEEE Trans. Wireless Commun.*, vol. 6, no. 4, pp. 1488–1500, april 2007.

[52] T. Schenk, *RF Imperfections in High-rate Wireless Systems.* Springer, 2008.

[53] T. Schmidl and D. Cox, "Robust frequency and timing synchronization for OFDM," *IEEE Trans. Commun.*, vol. 45, no. 12, pp. 1613–1621, Dec. 1997.

[54] T. Seki and N. Taga, "A novel phase noise suppression technique in OFDM receiver," in *International Conference on Consumer Electronics, ICCE 1998.*, Jun. 1998, pp. 388–389.

[55] W. Songping and Y. Bar-Ness, "Performance analysis on the effect of phase noise in OFDM systems," in *Proc. IEEE 17th International Symposium on Spread Spectrum Techniques and Applications*, vol. 1, 2002, pp. 133–138.

[56] ——, "OFDM systems in the presence of phase noise: Consequences and solutions," *IEEE Trans. Commun.*, vol. 52, no. 11, pp. 1988–1996, Nov. 2004.

[57] J. Stott, "The effects of phase noise in COFDM," *EBU Technical Review*, Summer 1998.

[58] L. Tomba, "On the effect of Wiener phase noise in OFDM systems," *IEEE Trans. Commun.*, vol. 46, no. 5, pp. 580–583, May 1998.

[59] R. Walden, "Analog-to-digital converter survey and analysis," *IEEE J. Sel. Areas Commun.*, vol. 17, no. 4, pp. 539–550, Apr. 1999.

[60] S. Weinstein and P. Ebert, "Data transmission by frequency-division multiplexing using the discrete Fourier transform," *IEEE Trans. Commun. Technol.*, vol. 19, no. 5, pp. 628–634, Oct. 1971.

[61] S. Wilson and J. Cioffi, "Probability density functions for analyzing multi-amplitude constellations in Rayleigh and Ricean channels," *IEEE Trans. Commun.*, vol. 47, no. 3, pp. 380–386, Mar. 1999.

[62] M. Windisch and G. Fettweis, "Performance degradation due to I/Q imbalance in multi-carrier direct conversion receivers: A theoretical analysis," in *IEEE International Conference on Communications, 2006*, Jun. 2006.

[63] ——, "Standard-independent I/Q imbalance compensation in OFDM direct-conversion receivers," in *In Proc. 9th Intl. OFDM Workshop InOWo*, 2004, pp. 57–61.

[64] S. Wu and Y. Bar-Ness, "A phase noise suppression algorithm for OFDM-based WLANs," *IEEE Commun. Lett.*, vol. 6, no. 12, pp. 535–537, Dec. 2002.

[65] E. Yonina Chana, "Quantum signal processing," PhD, Massachusetts Institute of Technology, Dept. of Electrical Engineering and Computer Science, 2002.